HHS Public Access

Author manuscript

Cell Rep. Author manuscript; available in PMC 2022 April 05.

Published in final edited form as:

Cell Rep. 2022 March 01; 38(9): 110436. doi:10.1016/j.celrep.2022.110436.

Structure-guided changes at the V2 apex of HIV-1 clade C trimer enhance elicitation of autologous neutralizing and broad V1V2-scaffold antibodies

Anusmita Sahoo[1,2], **Edgar A. Hodge**[3], **Celia C. LaBranche**[4], **Tiffany M. Styles**[1,2], **Xiaoying Shen**[4], **Narayanaiah Cheedarla**[1,2], **Ayalnesh Shiferaw**[1,2], **Gabriel Ozorowski**[5], **Wen-Hsin Lee**[5], **Andrew B. Ward**[5], **Georgia D. Tomaras**[4], **David C. Montefiori**[4], **Darrell J. Irvine**[6], **Kelly K. Lee**[3], **Rama Rao Amara**[1,2,7,*]

[1]Emory Vaccine Center, Yerkes National Primate Research Center, Emory University, Atlanta, GA 30329, USA

[2]Department of Microbiology and Immunology, Emory School of Medicine, Emory University, Atlanta, GA 30322, USA

[3]Department of Medicinal Chemistry, University of Washington, Seattle, WA 98195, USA

[4]Department of Surgery, Duke University Medical School, Duke University, Durham, NC 27710, USA

[5]Department of Integrative Structural and Computational Biology, The Scripps Research Institute, San Diego, CA 92121, USA

[6]David H. Koch Institute for Integrative Cancer Research, Massachusetts Institute of Technology, Cambridge, MA 02139, USA

[7]Lead contact

SUMMARY

HIV-1 clade C envelope immunogens that elicit both neutralizing and non-neutralizing V1V2-scaffold-specific antibodies (protective correlates from RV144 human trial) are urgently needed due to the prevalence of this clade in the most impacted regions worldwide. To achieve this, we introduce structure-guided changes followed by consensus-C-sequence-guided optimizations at the V2 region to generate UFO-v2-RQH^{173} trimer. This improves the abundance of well-formed

*Correspondence: ramara@emory.edu.

AUTHOR CONTRIBUTIONS

R.R.A. and A. Sahoo designed the study and wrote the manuscript. A. Sahoo performed experiments and analyzed data. E.A.H. did HIC purification, H/D exchange, and DLS experiments (supervised by K.K.L.). C.C.L. conducted neutralization assays (supervised by D.C.M.). T.M.S. did ADCVI. X.S. did BAMA assays (supervised by G.D.T.). G.O. and W.-H.L. did NS-EM (supervised by A.W.). A. Sahoo, N.C., and A. Shiferaw purified proteins and plasmids. A. Sahoo performed ELISA and BLI binding experiments. D.J.I. provided ISCOM.

DECLARATION OF INTERESTS

A patent has been filed on the C.1086 UFO trimers developed in the study, and R.R.A., A. Sahoo, and T.M.S. are co-inventors of this technology. The other authors declare no competing interests.

SUPPLEMENTAL INFORMATION

Supplemental information can be found online at https://doi.org/10.1016/j.celrep.2022.110436.

trimers. Following the immunization of rabbits, the wild-type protein fails to elicit any autologous neutralizing antibodies, but UFO-v2-RQH^{173} elicits both autologous neutralizing and broad V1V2-scaffold antibodies. The variant with a 173Y modification in the V2 region, most prevalent among HIV-1 sequences, shows decreased ability in displaying a native-like V1V2 epitope with time *in vitro* and elicited antibodies with lower neutralizing and higher V1V2-scaffold activities. Our results identify a stabilized clade C trimer capable of eliciting improved neutralizing and V1V2-scaffold antibodies and reveal the importance of the V2 region in tuning this.

In brief

HIV-1 immunogens that induce both neutralizing and V1V2-scaffold-specific antibody responses are needed to effectively protect against HIV infection. Sahoo et al. develop a clade C envelop immunogen capable of eliciting both of these responses and demonstrate the importance of the envelope V2 region in tuning immune outcome.

Graphical Abstract

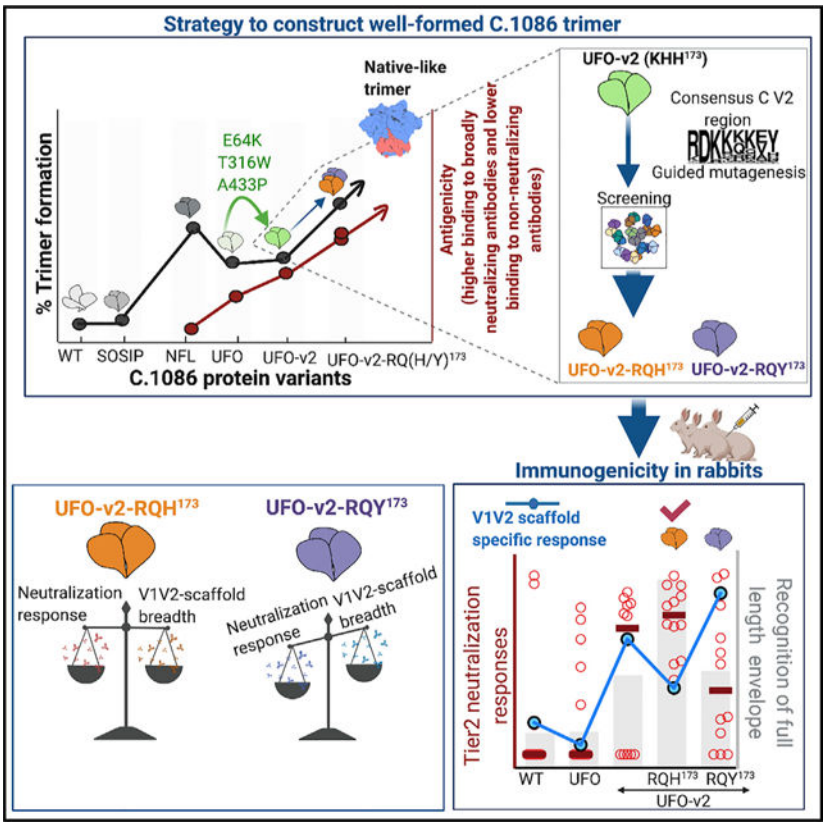

INTRODUCTION

The robust induction of HIV-1 envelope (env)-specific broadly neutralizing antibodies (bnAbs) by vaccination has been a major challenge. Strategies to stabilize the env protein in a closed trimeric conformation, such as SOSIP (Sanders et al., 2013), cleavage-independent native flexibly linked (NFL) (Sharma et al., 2015), un-cleaved prefusion optimized (UFO)

(He et al., 2018; Kong et al., 2016) trimeric designs, and “germline” bnAb precursor-targeting trimers (reviewed by McGuire, 2019) have advanced our efforts to successfully induce tier2 autologous nAbs (de Taeye et al., 2015; Escolano et al., 2016; Huang et al., 2020; Klasse et al., 2016; Pauthner et al., 2017; Sanders et al., 2015; Voss et al., 2017). However, these Ab responses generally had poor neutralization breadth, primarily directed toward epitopes specific to the immunizing env (Arunachalam et al., 2020; Bale et al., 2018; Dubrovskaya et al., 2017; He et al., 2018; Klasse et al., 2018; Pauthner et al., 2017; Sanders and Moore, 2017; Sanders et al., 2015; Torrents de la Pena et al., 2017). Exceptions include work by Xu et al. (2018) and Dubrovskaya et al. (2019), where broad nAbs were generated toward the fusion-peptide and cross-neutralizing responses toward CD4bs and gp120-gp41 interfaces, respectively. In addition to the nAbs, non-nAbs have been reported to contribute significantly toward protection in the RV144 trial, the only HIV vaccine efficacy human trial to date to show modest but significant efficacy (Rerks-Ngarm et al., 2009). In this trial, immunoglobulin G (IgG) responses generated toward HIV-1 env variable loops 1 and 2 (V1V2) scaffolded on MuLV gp70 protein (V1V2-scaffold), and a linear V2 epitope (residues 166–178, referred to as the V2 hotspot or the V2-HS region) (Tassaneetrithep et al., 2014) proximal to the α4β7 binding site correlated with decreased infection risk (Excler et al., 2014; Haynes et al., 2012; Rolland et al., 2012; Zolla-Pazner et al., 2013). Studies conducted in non-human primates (NHPs) have also emphasized the importance of V2-directed non-nAbs in delaying simian immunodeficiency virus (SIV) and simian-human immunodeficiency viruses (SHIV) acquisition (Barouch et al., 2012; Jones et al., 2019; Zolla-Pazner et al., 2014, 2019) and the passive transfer of anti-V2 mAbs (830A) in reducing viremia (Hessell et al., 2018). Protective responses associated with these non-nAbs are linked to Fc-mediated anti-viral effector functions and their ability to occlude interactions between the host integrin α4β7 and HIV-1 env to control and clear the virus (Gorny et al., 2012; Perez et al., 2017; Yates et al., 2014). Hence, the ability of an env immunogen to generate a broad V1V2 reactive response both in presence and absence of a strong cross-neutralizing response is an important parameter in immunogen design portfolios.

The design of an immunogen with the potential to elicit both tier2 neutralizing and broad V1V2-scaffold-specific binding Abs has not been explored. A closed, stabilized trimer designed to generate nAbs is less likely to expose the conformation presented by the V1V2 scaffolds, which are more flexible and lack the quaternary contacts, thereby making it difficult to design an immunogen with a fine balance in inducing both kinds of responses. Although studies have reported the significance of the V2 region in regulating the closed-state of the env and its neutralization sensitivity (Cimbro et al., 2014; Guzzo et al., 2018), understanding how these changes maintain native apex integrity with time, with/without impacting the trimer integrity is unexplored. How such changes affect the balance between induction of neutralizing versus a broad V1V2-scaffold-specific response is not known. We attempted to address these questions by engineering a stable clade C trimeric immunogen. In this context, clade C immunogens are critically needed since a large proportion (~48%) of the global HIV-1 burden results from viral infections within this clade (Geretti et al., 2009). We focused our efforts on C.1086 env, since its gp120 version was used in subtype-C adapted human phase 2b/3 HIV Vaccine Trials network (HVTN)702

trial (ClinicalTrials.gov: NCT02968849) (Gray et al., 2021). Although reasons for the trial's failure in preventing HIV-1 infection in participants are currently under investigation, the successful design of a stable C.1086 trimer capable of inducing improved neutralizing and broad V1V2-scaffold Abs will aid in its use under optimized vaccine regimens in future subtype-C-based SHIV challenge studies in NHPs and, if successful, in human clinical trials.

To this end, the wild-type (WT) C.1086 gp140 protein, which does not maintain well-formed trimer conformation, failed to induce autologous nAbs (Burton et al., 2019; Kasturi et al., 2017; Styles et al., 2019). Two studies made efforts to stabilize C.1086 in a well-formed trimeric form (Guenaga et al., 2017; He et al., 2018). A study by Guenaga et al. (2017) showed that the addition of glycine substitutions in the gp41 region of C.1086 NFL in combination with multiple trimer-derived changes improved the generation of well-ordered trimers. However, immunization studies with such stabilized trimers, specifically evaluating the generation of both neutralizing and broad V1V2-scaffold-specific Abs, have yet to be reported. Here, we adopted consensus clade C V2 hotspot (V2-HS, residues [res.] 166–173 in this study) sequence-guided mutational screening to design a C.1086 UFO-v2-RQH^{173} variant, which was capable of inducing improved autologous neutralizing and broader V1V2-scaffold-specific responses in rabbits. Further, the study results also highlighted the contribution of residues in the V2-HS region in altering the ability of the trimer to display a native-like V1V2 epitope with time without affecting trimer integrity *in vitro,* and influence the generation of neutralizing and V1V2-scaffold-specific responses in rabbits.

RESULTS

Screening of C.1086 base variants to select UFO form as the parent construct for stabilization strategies

As initial steps to generate a stable C.1086 trimeric protein, we generated the SOSIP, NFL (+I559P), and UFO (without disulfide linkage SOS between A501 and T605) variants (schematic shown in Figure 1A) and compared their ability to form trimers using size-exclusion chromatography (SEC). The proteins were expressed in 293F cells and purified by *Galanthus nivalis* lectin (GNL)-mediated affinity purification, followed by isolation of trimers by SEC. The majority of the SOSIP variants resulted in aggregates (only 23% trimer proportion) similar to the WT protein and were not characterized further (Figure 1B). Both NFL and UFO variants formed higher proportion of trimers (means of 61% and 50%, respectively; Figures 1B and 1C) relative to the SOSIP and WT proteins with net protein yields of 1.8 and 5.5 mg/L, respectively. In addition to a higher protein yield, the UFO form showed ~60-fold improved association kinetics against V1V2-apex-specific bnAb PG16 (Pejchal et al., 2010), resulting in a 44-fold improved binding (K_D UFO, 252 nM, NFL, 11μM; Figures 1D, 1G, and S1A; Table S1) against PG16 and comparable binding to other bnAbs (±3-fold) relative to NFL. This prompted us to select UFO as the parent design to further improve the trimer.

Structure-guided mutations in UFO backbone (UFO-v2) decrease exposure of non-neutralizing epitopes and binding to CD4

Although the UFO form improved binding to PG16, it did not reduce binding to non-neutralizing Abs relative to the NFL form (Figure 1D; Table S1). To minimize the exposure of non-neutralizing epitopes, we introduced three structure-guided mutations, T316W, E64K (de Taeye et al., 2015), and A433P (Kwon et al., 2015), that have been reported in the context of a BG505 SOSIP.664 trimer to improve hydrophobic interactions at the apex, restrict CD4-induced conformational changes, and reduce the exposure of the off-target V3 region. We named this variant UFO-v2 (Figure 1A). In previous studies, the WT and NFL-TD (i.e., NFL + "trimer-derived" TD stabilizing substitutions only) forms of the protein were reported to be insufficient in forming any well-formed trimers by negative-stain electron microscopy (EM) (Bontempo et al., 2020; Guenaga et al., 2017), while NFL-TD with additional stabilizing glycine substitutions in the HR1 region efficiently formed well-formed trimers (63% and 62% by EM, respectively) (Guenaga et al., 2017). Here, variants with and without stabilizing changes, i.e., UFO and UFO-v2 constructs, yielded >70% well-formed trimers by EM analyses (79% and 73%, respectively; Figures 1B and S2) and similar proportions of trimer fraction (50% for both variants; Figures 1B and 1C) based on their SEC profiles. However, UFO-v2 displayed markedly reduced binding to V2i 697-30D non-nAbs (70-fold) and other non-nAbs (447-52D, 39F, and CH58; 6-, 14-, and 5-fold decrease in K_D, respectively) along with no apparent binding to CD4i 17b and 48d non-nAbs relative to UFO, supporting the reduced exposure of non-neutralizing epitopes (Figures 1E and 1F). The absolute affinity of UFO-v2 measured against non-nAbs is still high, and other stabilization strategies are required to further reduce this. UFO-v2 also displayed reduced binding to CD4-IgG2, which, however, did not affect recognition by CD4-binding site bnAb NIH-45-46^{G54W} (Figures 1E, 1F, and S1A; Table S1), likely due to E64K substitution, which has been reported previously to reduce binding to CD4 (Liu et al., 2017). Both UFO and UFO-v2 exhibited similar binding (±3-fold change in affinity) to neutralizing Abs (Figures 1E and 1G; Table S1). Thus, structure-guided mutations introduced in the backbone of a C.1086 UFO (i.e., UFO-v2) trimer decreased the exposure of non-neutralizing epitopes.

Sequence-guided mutations at V2-HS region improve antigenicity of the V2 apex on C.1086 trimers

Despite the minimized exposure of non-neutralizing epitopes, the UFO-v2 protein exhibited moderate affinity toward V1V2-apex-specific bnAbs (K_D > 100 nM; Figures 1G and S1A; Table S1). In order to improve binding to this class of bnAbs and thereby stabilize the protein into a closed well-formed trimer, we optimized the V2-HS region (res 166–173 in the present study) on env carrying the signature binding residues to V1V2-apex-specific bnAbs (Bricault et al., 2019). To do this, we identified four positions, 166, 170, 172, and 173, in C.1086 (UFO-v2) that differed from the clade C consensus V2-HS region (n = 22,415 sequences; Figure 2A) and substituted them with either dominant or sub-dominant amino acids present in the consensus sequence as single, double, triple, or quadruple mutants (listed in Figure 2B, left). These mutants (referred to as UFO-v2 V2-HS mutants) were screened initially by ELISA to identify variants that enhanced binding to PGT145 and other V1V2-targeting bnAbs. We observed that all designs bearing K166R significantly improved binding to PGT145 with minimal effects on binding to other env-specific Abs

(Figures 2B and S3A). The result was justified, as the previously solved structure of BG505 SOSIP.664-PGT145 (PDB: 5V8L [Lee et al., 2017]) showed direct interaction between arginine at the 166 position and PGT145 HCDR3 loop and its preference for recognition by V1V2-apex-directed bnAbs (Bricault et al., 2019). V2-HS mutants K166R/H170Q/H173 (UFO-v2-RQH^{173}) and K166R/H170Q/H173Y (UFO-v2-RQY^{173}) showed the strongest binding to PGT145 (Figures 2B and S3A) and, hence, were studied further. The K166R and H170Q V2-HS changes enhanced the proportion of C.1086 trimers (Figures 2C, left, and S3B). Similarly, a more distant clade A BG505 SOSIP.664 protein that has 166R and 170Q residues in the WT sequence, displayed a reduction in the trimeric proportion when these residues were changed to those present in the WT C.1086 sequence (Figures 2C, right, and S3B). This suggested a plausible role of 166R and 170Q in improving the folding of the env protein and, thereby, forming higher proportion of trimers. The C.1086 UFO-v2 V2-HS-purified proteins majorly folded into trimers, which was evident by blue native PAGE (BN-PAGE; Figure 2D) and EM (Figure S2). We anticipate that additional purification steps involving anion-exchange, hydrophobic interaction chromatography (Verkerke et al., 2016), and bnAb- and non-nAb-based positive and negative selections (Guenaga et al., 2015) would likely further improve the purity of the trimers. The purified trimers displayed 5- to 6-fold improved binding to PGT145 (average K_D: 34 nM; Figures 2E, 2F, and S1A; Table S1) compared with the parent UFO-v2 that had no significant changes in affinity (±3-fold) toward other env-specific mAbs (Figure 2F; Table S1) by bio-layer interferometry (BLI). Binding affinities measured against V1V2 bnAbs PGT145 and PGDM1400 (Sok et al., 2014) (Table S2) were similar to those reported previously for the stabilized C.1086 NFL-TD variant (K_D: 41 nM for PGT145 and 40 nM for PGDM1400 [Guenaga et al., 2017]), suggesting UFO-v2 V2-HS as an alternative strategy for stabilizing the C.1086 trimer. Previous studies have highlighted the enhanced sulfation of Tyr at 173 position to increase recognition by trimer-specific bnAbs (Cimbro et al., 2014). Here, we did not observe the sulfation of 173Y in C.1086 UFO-v2-RQY^{173} when analyzed by tandem mass spectrometry (MS/MS) electron-transfer/higher-energy collision dissociation (EThcD) experiments (Yu et al., 2017). Both 173 variants UFO-v2-RQ(H and Y)^{173} displayed similar Ab binding profiles (Table S1; Figure 2D). In summary, consensus C V2-HS sequence-guided changes, specifically K166R introduced to generate UFO-v2-RQ(H/Y)^{173} trimers, enhanced binding to V2-specific PGT145 bnAbs.

C.1086 UFO-v2-RQ(H/Y)^{173} trimers bear a highly dynamic V1V2 loop and show differences in their resilience to display V1V2 bnAb-reactive epitopes with time

To identify any potential structural differences between C.1086 UFO-v2-RQ(H/Y)^{173} trimer variants, we measured their backbone dynamics with hydrogen-deuterium exchange MS (HDX-MS) experiments. To eliminate spurious signals in the HDX-MS experiment, we repurified the proteins with hydrophobic interaction chromatography (HIC) to obtain highly monodisperse trimers. Both C.1086 UFO-v2-RQ(H/Y)^{173} trimers displayed similar HDX profiles for the peptides we could monitor, including res. 176–179 (proximal to 173 position) in the V2 region, indicating no differences in the global and local structural organizations of the UFO-v2-RQ(H/Y)^{173} trimers, which was indeed consistent with their similar antigenic profiles (Figure S4; Table S1).

A BG505 SOSIP.664 trimer was used as a reference for HDX-MS experiments due to its extensive structural characterization in previous studies (de Taeye et al., 2015; Guttman et al., 2014). The homologous peptic peptides between C.1086 and BG505 envs present at the gp120-gp41 interface; res. 35–52 and 484–501 were observed to be protected (Figures S4, 3A, and S5A), which indicated that the trimers were well-folded (Verkerke et al., 2016). The C.1086 UFO-v2-RQ(H/Y)^{173} trimers showed overall high local structural dynamics at the apex and in portions of gp41 (Figures S5B, and 3A) and also relative to BG505 SOSIP.664 trimer (Figures 3A, S5A, and S4). Notably, the base of V1 ^{112}WDESLKPCVKLTPL^{126} and the peptide segment ^{176}FYKL^{179} present in the V2 loop of env was found to be more dynamic in C.1086 UFO-v2-RQ(H/Y)^{173} than in the BG505 SOSIP.664 trimer, which is known to have a well-ordered V1V2 apex (Figures 3A, S5A, and S4). The C.1086 ^{176}FYKL^{179} was the most dynamic (Figures 3A and S4). The increased flexibility of the V2 loop in the C.1086 UFO trimer compared with the BG505 SOSIP.664 trimer was further suggested by the enhanced binding of mAb CD58 (Liao et al., 2013) to the former compared with latter (Bontempo et al., 2020), which recognizes a linear V2 epitope generally displayed on a more flexible V2 antigen such as the gp70-V1V2 scaffold that lacks the native display of variable loops (Figure S1B). As expected, CH58 bound to the gp70-C.1086 V1V2 scaffold with a higher affinity than C.1086 UFO-v2 V2-HS trimers (Figures S1B and S1C).

Additionally, we were interested in probing whether residue alterations in the V1V2 region, here, 173H and 173Y changes, could influence the native integrity of the V1V2 apex of a trimer with time. To address this, we incubated UFO-v2-RQ(H/Y)^{173} immunogens at 25°C for 0 to 15 h and measured any change in binding kinetics against different mAbs scanning various epitopes on the trimer (Figure S5D), relative to time 0 (baseline). We noticed the largest reduction in binding affinity of the trimers to the V1V2 apex targeted bnAbs after 12 h relative to other immunodominant epitopes targeting mAbs (bnAbs PGT151, NIH45-46, and PGT121; non-nAbs F105, 447-52D, 39F, and 697-30D), which, in contrast, were marginally affected (<3-fold reduction; Table S2; Figure 3B). Specifically, UFO-v2-RQY^{173} showed a dramatic reduction in binding affinity toward V1V2-specific PG16 (mean of 52-fold), PG9 (mean of 19-fold), and CAP256-VRC26.08 (mean of 5-fold) bnAbs as early as within 4 h of incubation, in contrast to no significant (<2-fold) reduction observed for UFO-v2-RQH^{173} (Figure 3B; Table S2). Similar observation was noted for UFO-v2-RQY^{173} relative to UFO-v2-RQH^{173} against other V1V2 bnAbs, PGT145, PGDM1400, and V2p CH58 after 12 and 4 h of incubation, respectively. This time-dependent significant reduction in affinity of UFO-v2-RQY^{173} versus UFO-v2-RQH^{173} was observed to be driven by significantly reduced association rates, without much change in the dissociation rate (Figure S5C; Table S2). Epitopes on the trimer showing reduced accessibility to Abs after prolonged incubation included V2 B-C β-strands carrying the binding footprint of the V1V2-apex-specific bnAbs (Bricault et al., 2019) and a V2 C β-strand on the trimer harboring the linear V2 epitope recognized by CH58 V2p non-nAbs but in a helix/coil conformation (Liao et al., 2013) (Figures S5D–S5F). The V2 C β-strand harbors the 173 position (Figure S5E). Here, the 173Y trimer variant demonstrated reduced durability in displaying the epitope reactive to V1V2 bNAbs with time compared with UFO-v2-RQH^{173} *in vitro,* although the two C.1086

UFO-v2-RQ(H/Y)^{173} variants displayed similar Ab binding profiles for V1V2-apex-specific bnAbs (Table S1) at baseline time 0.

In summary, the C.1086 trimers (UFO-v2-RQ(H/Y)^{173}) exhibited higher V2 loop dynamics and accessibility relative to the well-characterized BG505 SOSIP.664 trimer. His and Tyr V1V2 point variants at the 173 position of C.1086 trimers displayed overall similar structural dynamics but exhibited differences in their resilience to display the V1V2 epitope accessible to native apex-targeting bnAbs overtime *(in vitro)* without any effect on the trimer integrity.

C.1086 UFO-v2 variants induce higher trimer-specific responses in rabbits

We next investigated if the modifications introduced in C.1086 UFO designs could improve immune responses induced by vaccination relative to the WT protein and also influence the quality of responses (will be discussed in subsequent sections), given the observations that the C.1086 trimer carried a highly dynamic V1V2 loop and UFO-v2-RQ(H/Y)^{173} variants exhibited differences in time-dependent V1V2 epitope stability. To this end, we vaccinated female New Zealand rabbits (10–12 weeks old, n = 4 per group) subcutaneously with either (1) WT, (2) UFO, (3) UFO-v2, (4) UFO-v2-RQH^{173}, or (5) UFO-v2-RQY^{173} proteins (30 μg each immunization, 375 U immune-stimulating complex [ISCOM] as adjuvant) at weeks 0, 8, 24, and 40 and bled them 2 weeks after each immunization to characterize their serum responses (Figure 4A). All rabbits, regardless of immunization group, elicited similar binding Ab responses against WT C.1086 gp140, which was monitored 2 weeks after the final boost (Figure 4B, left). All groups manifested moderate (ranging 10^4–10^6 ELISA endpoint titers without outliers) trimer-specific Ab responses after the first immunization, followed by a maximum of a 237-fold average boost in responses after the second protein, and a 14- and 27-fold average boost after the third and fourth proteins, respectively (Figure S6A). All UFO-v2 variants induced higher trimer-specific binding Abs than did WT; specifically, UFO-v2-RQH^{173} and UFO-v2-RQY^{173} groups displayed 39-fold higher responses ($p = 0.03$ with respect to WT in each case; Figures 4B, right, and S6B). Although all groups, including WT, induced comparable responses against the unwanted V3 peptide (Figure 4C, left), we observed significantly lower V3 responses normalized to the total trimer-specific responses in all UFO backbone-bearing groups relative to WT (Figure 4C, right). Similar levels of V3-specific Abs were observed in UFO-v2-RQH^{173} and UFO-v2-RQY^{173} groups, which was supported by similar V3 backbone dynamics (^{318}YATGDIIG^{324} region) of the proteins monitored by HDX experiments (Figure S4). In summary, higher proportions of trimer-specific binding Abs were induced by all C.1086 UFO-v2 variants in rabbits.

UFO-v2-RQH^{173} induces highest anti-viral Ab responses and binding Abs to membrane-anchored tier2 envs

We investigated if the changes introduced in the designs influenced (1) the generation of neutralizing Abs and (2) the recognition of membrane-anchored diverse tier1 and tier2 full-length envs. In addition, we were interested in understanding if differences at the 173 position, i.e., H or Y (as in UFO-v2-RQH^{173} and UFO-v2-RQY^{173}) would influence the nature of immune responses generated (this will be discussed below for clarity). We

assayed nAb responses against homologous and heterologous tier2 pseudotyped envs and their binding to membrane-anchored gp160s constituting the tier1 and tier2 global panels. We used purified IgG to eliminate sporadic low-level background and to be sure that the activity was mediated by IgG. IgG from all animals showed strong nAb titers against tier1 env MW965.26 (Figures 4D, 4E, right, and S6C; Table S3). C.1086 WT has been previously found to be inefficient in eliciting homologous neutralization titers (Kasturi et al., 2017; Styles et al., 2019). IgG from WT and UFO-immunized animals induced only sporadic clade C tier2 responses and increased only marginally in UFO-v2-immunized animals. However, UFO-v2 V2-HS changes in UFO-v2-RQH^{173} resulted in the induction of overall better neutralization titers against homologous (C.1086 K160N RQH^{173} and C.1086 K160N RQY^{173}) and heterologous (25710) pseudotyped viruses than WT and UFO did in a combined analysis ($p = 0.003$ and 0.0006, respectively) (Figures 4D and 4E, left). Additionally, groups immunized with UFO variants showed sporadic induction of moderately better neutralizing responses against the tier2 X1632 (clade G) pseudovirus than the WT (Table S3). Weak/negligible responses was measured for all groups against other tier2 pseudoviruses tested (Table S3).

In an attempt to evaluate the ability of the serum to recognize diverse full-length envs, we monitored the binding of purified serum IgGs to 293T cells expressing membrane-anchored gp160, including the tier1 and tier2 global panels (deCamp et al., 2014) of envs (representative plots in Figure S6D). Reactivity to the env panel was poor in WT and UFO groups and increased significantly in UFO-v2 and UFO-v2-RQH^{173} groups, with UFO-v2-RQH^{173} showing the highest responses (Figure 4F). As anticipated, the serum Ab binding responses to membrane-anchored envs correlated positively with the neutralization responses measured against corresponding pseudotyped envs (Figure 4G). Also, C.1086 trimer-reactive serum Abs correlated positively with binding responses measured against their full-length gp160 forms ($p = 0.002$; Figure S6E), suggesting immunization with optimized C.1086 trimers to help in the generation of Abs recognizing full-length envs. In total, these results demonstrated the UFO-v2 changes introduced to stabilize the trimer resulted in induction of better autologous neutralizing and cell-surface env-binding Ab responses relative to WT protein, and the V2-HS changes K166R and H170Q in UFO-v2 (i.e., UFO-v2-RQH^{173}) further enhanced these responses.

173Y modification in UFO-v2-RQH^{173} marginally reduces induction of functional Ab responses

To understand the contribution of 173Y in the induction of functional Ab responses, we compared neutralizing, Ab-dependent cell-mediated virus inhibition (ADCVI) and the cell-surface env-binding activity of IgGs purified from the UFO-v2-RQY^{173} group. In all cases, we observed a modest decrease in responses in the UFO-v2-RQY^{173} group compared with in the UFO-v2-RQH^{173} group (Figures 4D, 4E, left, 4F, and 4H), indicating that 173Y modification can negatively influence the induction of functional Ab responses in the context of UFO-v2-RQH^{173}. This observation prompted us to investigate if 173Y would be selected over 173H in natural HIV-1 isolates, as it elicited weaker anti-viral responses. To address this, we analyzed the V2-HS region (res 166–173) of clade C consensus sequences from tier1, tier2, and tier3 isolates categorized by Rademeyer et al. (2016). We observed

increased occupancy of highly conserved Tyr and reduced occupancy of the sub-dominant His residue at 173 position as the tier level (or the difficulty level to neutralize the virus) increased from tier1 to tier3 (Figure 4I; tier1: Y 60% and H 15%, tier2: Y 67% and H 9%, tier3: Y 77% and H 7%). These data corroborated with the possible selection of Tyr at the 173 position in the viral envs to increase its chances to escape the immune system by decreasing its tendency to elicit anti-viral responsive Abs, relative to 173H. The presence of Tyr or His at the 173 position in the backbone of the C.1086 env did not influence its infectivity, in the absence of any immune pressure (Figure S6F). It will be important to monitor infectivity of the variants in other cell types. It should be noted that the sequence analysis was limited by the number of tier-categorized clade C sequences available, and 173 was not the only position being influenced by the tier level. In summary, the choice of residue (here, H/Y) at the 173 position in C.1086 UFO-v2-RQ(H/Y)^{173} trimers was capable of tuning the generation of Abs with anti-viral functions, which is an important implication for vaccine design.

173Y modification in UFO-v2-RQH^{173} enhances the breadth of V1V2-scaffold-specific responses

To evaluate the ability of the C.1086 variants to induce broad V1V2 scaffold responses, we assayed the binding of the serum to gp70-V1V2 scaffold proteins from 16 HIV-1 strains spanning diverse clades by binding antibody multiplex assay (BAMA) (Zolla-Pazner et al., 2014) in addition to monitoring this against the homologous strain by ELISA. Rabbits immunized with the UFO variants induced higher homologous V1V2-scaffold-specific responses than the WT protein; the highest titers (measured by ELISA) were seen in the UFO-v2 V2-HS groups (Figure 5A). All immunogens generated cross-reactive V1V2-scaffold-specific Abs (Figures 5B and S6G), which were overall significantly higher and broader in all UFO-v2 variants than in the WT (Figure 5C). Interestingly, UFO-v2-RQY^{173} elicited markedly higher V1V2-scaffold-specific responses (Figure 5B), with higher recognition breadths ($p < 0.001$; Figure 5C) than UFO-v2-RQH^{173}. The results indicated favorable contributions of UFO-v2 in enhancing the cross-reactive V1V2-scaffold breadth, which was further enhanced by 173Y in combination with the V2-HS changes (K166R/H170Q). The high V2 loop dynamics and accessibility of this region on C.1086 trimers, as measured by HDX-MS, may potentially explain the ability of C.1086 UFO-v2 well-formed trimers to elicit Abs that show a broad range of V1V2-scaffold binding. Additionally, lesser time-dependent V1V2 epitope stability of UFO-v2-RQY^{173} relative to UFO-v2-RQH^{173} may potentially explain the higher scaffold V1V2 recognition breadth of UFO-v2-RQY^{173} immunized serum relative to its counterpart. Serum Ab responses measured specific to gp70 V1V2-scaffold envs correlated positively with binding responses specific to corresponding membrane-anchored envs (Figure S6I). It should be noted that the overall frequency of env^{+} cells showing binding to serum IgG was low compared with the frequency of env^{+} cells showing binding to PGT121, PGT145, and PG16 bnAbs (Figure S6H). The lower frequencies of env^{+} cells are expected with polyclonal sera compared with high-affinity monoclonal Abs.

Principal-component analysis (PCA) of the immunogenicity data segregated UFO-v2-RQH^{173} and UFO-v2-RQY^{173} into two separate clusters, implying true differences in

immune responses elicited due to changes at the 173 position (Figure 5D). V2-HS changes and optimizations in the presence of 173Y (UFO-v2-RQY^{173}) did not seem to additionally influence immunogenicity and thereby clustered (rabbit #537 being the outlier) with the ancestor UFO group, unlike UFO-v2-RQH^{173}, which clustered separately from both UFO and UFO-v2 groups. The most notable variables significantly ($p < 0.05$) contributing toward these differences in PCA responses were the binding to V1V2 scaffolds of tier2 homologous and heterologous envs, membrane-anchored tier2 25710 env and neutralization against 25710 pseudotyped virus (Figure S6J). Overall, these data suggested an important role of V2-HS residues, particularly the 173 position in modulating the immune responses, with the nature of the residue as the governing player.

Trimer stabilizing modifications induce Abs that compete with CD4bs-specific bnAbs

To gain insights into the epitope specificity of the Ab responses induced by the immunogen/trimer modifications, we performed competition binding experiments between rabbit serum and a panel of well-characterized bnAbs by BLI (representative responses shown in Figure 6A). We observed the generation of CD4bs-specific Abs in all UFO-v2 backbone-bearing groups competing with NIH45-46^{G54W} and modestly competing with HJ16 in rabbits with a half maximal inhibitory concentration (IC_{50}) <400 μg/mL (Figure 6B). The percentage of competition with NIH45-46 correlated positively with the homologous C.1086 neutralization IC_{50}, the concentration of IgG required for 50% neutralization of the pseudovirus ($p = 0.002$, $r = -0.6$; Figure 6C). These results demonstrated early signs of the plausible presence of CD4bs neutralizing Abs in the serum. To probe residue-wise binding/neutralization specificity of the Abs, we created a series of CD4bs mutants in C.1086 K160N RQH^{173} background: N279Q, N280D, S365K, I371A, G458Y, G459(E/P); only N279Q and N280D yielded infectious units. We observed reduced neutralization of N279Q (in a few) and N280D knockout (KO) mutant viruses (5-fold median reduction in IC_{50} relative to parent C.1086 K160N RQH^{173} in all purified IgGs tested, regardless of the immunization group; Table S3). This suggested the presence of CD4bs Abs in the serum that were different from the VRC01 class of bnAbs (VRC01-class CD4bs bnAb activity is dependent on N280 [Lynch et al., 2015]); further analyses are needed to identify the fine specificity of the neutralizing activity in these sera. Interestingly, rabbit #537 (IC_{50} against C.1086 RQH^{173} = 173 μg/mL) immunized with UFO-v2-RQY^{173} seemed to have elicited V1V2-specific Abs competing against prototype PG16 (99%), PG9 (86%), VRC26.09 (64%), PGDM1400 (54%), and PGT145 (48%) bnAbs besides eliciting CD4bs-specific Abs in the serum (Figures 6B and 6C). None of the rabbits elicited V3-glycan-specific (PGT121-like) Abs. Most rabbits bearing CD4bs bnAb epitope specificity also exhibited non-neutralizing V3- (39F-like), V2p- (CH58-like) and V2i- (697-30D) targeting Abs. The CAP228-16H V2p Ab recognizes both 173H- and 173Y-bearing V2 peptides, unlike CH58, and exhibit potent antibody-dependent cell-mediated cytotoxicity (ADCC) activities (van Eeden et al., 2018). Encouragingly, our data suggested the presence of CAP228-16H-like Abs in all rabbits vaccinated with UFO-v2-RQH^{173}, in contrast to only one out of four rabbits (rabbit #537) in the UFO-v2-RQY^{173} group. Overall, the stabilized UFO variants were able to induce CD4bs-directed, and one instance of V1V2-binding Abs which competed for binding with bnAbs specific for those epitopes.

DISCUSSION

Here, using structure- and sequence-guided strategies, we engineered the C.1086 env protein to form well-folded, stable gp140 trimers that elicit Abs in rabbits with improved functional tier2 anti-viral activities and broad V1V2-scaffold-specific binding responses compared with WT proteins, where past attempts using WT variants were reported to be inefficient in eliciting any homologous nAb responses (Burton et al., 2019; Kasturi et al., 2017; Styles et al., 2019). The SOSIP variant of C.1086 mostly yielded aggregates, as observed earlier for other env sequences (Guenaga et al., 2015), while the NFL and UFO forms generated higher fractions of trimers with better binding to some of the bnAbs. In addition, the UFO form showed better binding to PG16, and the introduction of the structure-guided mutation A433P in combination with E64K/T316W (UFO-v2 variants) significantly reduced binding to non-nAbs while preserving strong binding to nAbs and trimer integrity. Furthermore, our results showed that the V2-HS stabilization changes of Arg at position 166 markedly enhanced binding to PGT145 and, together with Glu at position 170, improved the fraction of C.1086 trimers. As these V2-HS changes were derived from a consensus C sequence, they are likely to translate to other envs. This was evident by their effect on improving the proportion of trimers in case of a more distant and well-characterized clade A BG505 SOSIP trimer. Together, our results identified critical residues that regulate the formation of stabilized trimers of a clade C protein and highlighted the contribution of amino acids in the V2-HS for improving trimer formation and antigenicity for V2-directed bnAbs.

Our results showed that the stabilization of C.1086 env trimers resulted in the induction of Ab responses in rabbits that bind better to trimeric proteins and recognize multiple tier2 envs expressed on the cell surface. The UFO-v2 variant with His at position 173 in the V2-HS region induced the highest nAb response. The stabilization also markedly improved the induction of Ab responses with broad reactivity against diverse V1V2-scaffold proteins. The stronger induction of nAb responses with greater stabilization of the protein was expected; however, a stronger induction of V1V2-scaffold binding Ab responses was unexpected, since the V1V2 scaffolds do not present the V1V2 loops in native conformation. Mechanistically, our results showed that the V1V2 loops in C.1086 UFO-v2 trimers were more dynamic relative to the BG505 SOSIP trimer, which is known to have a well-structured V1V2 apex and, hence, may be a potential factor responsible for the induction of broad V1V2-scaffold binding Abs by stabilized C.1086 UFO-v2 variants.

Previous studies have shown that substituting Tyr at the 173 position of the HIV env to either Ala or Phe altered neutralization sensitivity specific to an “open” conformation (Cimbro et al., 2014; Guzzo et al., 2018), suggesting the important role of the 173 position in regulating native env conformation. Located in the V2 C β-strand, residue 173 is adjacent to N156 and its associated glycan, which is spatially proximal to glycan at N160. N156 has been shown to be involved in recognition by V2-apex-targeting bnAbs, including PG16 and PGT145 (Lee et al., 2017; Pancera et al., 2013). Loss of N156 GlcNAc on the env has been reported to alter the inter-V2 strand interaction and form aberrant trimers (Lee et al., 2017) and non-infectious pseudovirus particles (data not shown). Here, though the amino acid type at the 173 position of C.1086 UFO-v2-RQ(H/Y)^{173} trimers did not alter the local structural order of proximal peptides (“FYKL” res. 176–179) monitored by HDX-

MS, it is conceivable that the side-chain choice at the 173 position might influence the disposition of the glycan chain at N156 and its associated interactions with the V1V2 trimer-specific bnAbs. Based on time-dependent BLI data, where UFO-v2-RQH^{173} displayed higher durability in maintaining the V1V2-apex-specific antigenicity for an extended time period *in vitro* relative to UFO-v2-RQY^{173}, 173H is likely to favor this interaction over 173Y in the context of C.1086 UFO-v2-RQ(H/Y)^{173} trimers. Additionally, it is possible that the amino acid type at this position may influence the ability of well-formed trimers to form higher order oligomers, such as larger assemblies of trimers, when the proteins are incubated at 25°C for an extended time period and occlude/alter accessibility of the V1V2 epitope for recognition by V1V2 trimer-specific bnAbs. Such an interaction would be consistent with the formation of larger and more heterogeneous species over time by UFO-v2-RQY^{173}, as monitored by dynamic light scattering (DLS) at 25°C at a relatively higher frequency than UFO-v2-RQH^{173} (data not shown) and agree with the time-dependent V1V2 trimer-specific affinity differences, particularly against PGT145 measured for the proteins. These structural differences, as one of the potential factors, may help explain some of differences in immune responses observed for the 173 position variants *in vivo* in this study. Accessibility of the V1V2 quaternary epitope present at the apex of the trimer could influence the induction of Abs with anti-viral functional activities (e.g., neutralization, ADCVI, and ADCC responses), V1V2-scaffold-specific binding responses, and the protective efficacy of the immunogen in an animal challenge study. Increased V1V2-scaffold Abs have been correlated with a reduced risk of viral acquisition and anti-viral activities, e.g., ADCC. However, the UFO-v2-RQY^{173}-immunized group, exhibiting the highest V1V2-scaffold binding Abs, showed minimal anti-viral ADCVI activity. This could be due to (1) differences in the assays or (2) the nature of the V1V2-scaffold Abs induced by 173Y and other studies, including those generated by the 173H variant which needs in-depth study.

The RV144 vaccine regimen included priming with a canarypox vector, the ALVAC-HIV-expressing subtype AE env, and boosting with bivalent subtype B/E gp120s. To measure the immune responses elicited by the RV144 trial regimen in South Africa, HVTN097 (Gray et al., 2019) and HVTN100 (Bekker et al., 2018) clinical trials were conducted. The HVTN097 study used the same clade AE and B/E env immunogens that were used in the RV144 vaccine regimen, and the protein was adjuvanted with Alum. The HVTN100 study also used the RV144 regimen but with subtype-C-based immunogens (C.1086 and TV1), and the protein was adjuvanted with MF59. Recent evaluations (Shen et al., 2020) of the responses elicited by both studies showed that the HVTN100 trial elicited a higher binding Ab response to homologous V1V2 scaffolds than the HVTN097 trial. Despite this, the V1V2-scaffold binding to heterologous clade C envs in the HVTN100 was significantly lower than that induced by the HVTN097 sera. These results indicated that the clade C gp120s used in the HVTN100 trial possibly lacked the ability to induce broad V1V2 reactive responses, which were important immune correlates of protection in the RV144 trial. In this context, our results showed that the C.1086 trimer, whose V2-HS region was modified based on the consensus C sequence, displayed improved induction of Abs reactive to V1V2 scaffolds both in terms of magnitude and breadth. This emphasizes the importance of optimizing the V2-HS region of immunogens in future clinical trials to induce broad V1V2-specific Abs.

To evaluate the efficacy of the HVTN100 vaccine regimen, the HVTN702 phase IIb/III trial (Gray et al., 2021) was conducted. Unfortunately, the HVTN702 trial failed to show any vaccine efficacy, and multiple factors could have contributed to the failure. One possible reason could be due to the lack of generation of strong and broad V1V2-scaffold-reactive Ab responses by the C.1086 gp120 immunogen. Another important difference between the RV144 and HVTN702 trials was the adjuvant used with protein immunizations: alum was used in the former, and MF59 in the latter. Coincidentally, an NHP study that evaluated the RV144 regimen with alum and MF59 as adjuvants using SIV immunogens and SIV challenge showed protection with alum but not MF59 (Vaccari et al., 2016). However, more work and analyses will be required to understand the mechanisms that contributed to the failure of HVTN702.

The next steps for the clinical translation of the results from rabbits to humans will be to test if these optimized clade C env immunogens elicit strong and broad nAb and V1V2-scaffold responses in NHPs, and if they enhance protection against heterologous clade C SHIV challenge. If successful, the immunogens can be advanced for human testing. In this regard, our data also showed the contribution of the optimized V2-HS changes in enhancing the expression levels of the trimer and in improving the neutralization potency of the immune responses elicited, which are added advantages to the immunogen. The optimized trimer was stable at 25°C for at least 24 h. In total, the C.1086 trimer developed in this study displayed multiple benefits to serve as guide for the design of immunogens in clinical translational studies.

In summary, we generated a clade C C.1086 trimer capable of simultaneously inducing functional autologous tier2 virus-reactive Abs as well as broad V1V2-scaffold-specific responses in rabbits. In addition, our results highlighted the influence of V2 residues His or Tyr at the 173 position in altering the durability in displaying V1V2 epitopes reactive to V1V2 bNAbs with time *in vitro,* and in combination with the highly dynamic V1V2 region of C.1086 trimers modulated the induction of V1V2-scaffold and functional Ab responses. Identification of 173(H/Y)-like residues by high-throughput screening and sequence analyses across various regions of the env surface may improve our fundamental understanding of linking the relationship between fine-tuned antigen design and immune outcome.

Limitations of the study

The findings of the study are limited to immunogens designed using only the C.1086 env and hence require an extension to multiple clade C and cross-clade envs to score generalizability of the findings. Additionally, conducting the study with a higher number of animals will strengthen the study findings. Vaccine-specific Abs generated in different model organisms differ from each other (Escolano et al., 2021). Thus, as discussed above, it will be important to measure the immune responses elicited by the V2-HS variants of the optimized C.1086 env in NHPs and compare the results with those obtained in the present study.

STAR★METHODS

RESOURCE AVAILABILITY

Lead contact—Further information and requests for resources and reagents should be directed to and will be fulfilled by the lead contact, Prof Rama Rao Amara (ramara@emory.edu).

Materials availability—All unique mutant plasmids generated in this study may be requested from the authors with a completed Materials Transfer Agreement.

Data and code availability

- Native gel image reported in the manuscript has been deposited at Mendeley, https://doi.org/10.17632/9zp2hh598z.1. 2D class average image of purified C.1086 gp140 variants by negative-stain electron microscopy has been included in the manuscript supplementary data. The raw data will be shared by the lead contact upon request.
- The study did not generate/analyze any dataset/code and does not report any original code.
- Any additional information required to reanalyze the data reported in this paper is available from the lead contact upon request.

EXPERIMENTAL MODEL AND SUBJECT DETAILS

Animal subjects—Female New-Zealand white rabbits (10–12 weeks old, n=4 per immunization group) were used in the study. The rabbits were housed and immunized at Covance Laboratories, Inc., Denver, PA, USA in compliance with IUCUC protocol 0065–18.

Microbial, viral strains and primary cell culture—NEB® 5-alpha E. coli (NEB), NEB® Stable Competent E. coli (NEB) cells were used for transformation and plasmid preparations as indicated in the Methods. The cells were grown at 37°C and 30°C respectively. Tier2 Clade C SHIV 1157ipD3N4 was generously provided by Dr. Ruth Ruprecht and the HIV reagent resource. The virus stock was stored in liquid N2, and thawed on ice for use as required. HEK 293T (American Type Culture Collection, ATCC) and TZM-bl cells (NIH AIDS Reagent Program) were grown in DMEM medium supplemented with fetal bovine serum (10%), penicillin (100U/ml), streptomycin (100μg/ml), and L-glutamine (2mM), incubated at 37°C, 5% CO2. CEM-NK^{r} CCR5^{+} (NIH AIDS Reagent Program) cells were grown in RPMI medium supplemented with fetal bovine serum (10%), HEPES (25mM), primocin (100μg/ml), and L-glutamine (2mM), incubated at 37°C, 5% CO2.293F cells were grown in Expi293™ Expression Medium, incubated at 37°C, 8% CO2, 130 rpm.

METHOD DETAILS

Immunizations in rabbits—Five C.1086 immunogens viz. WT, UFO, UFO-v2, UFO-v2-RQH^{173}, UFO-v2-RQY^{173} were tested for their immunogenicity responses in female New-Zealand white rabbits (n=4 per group). Each rabbit was immunized subcutaneously with group specific protein (30μg/dose) on the neck (dorsal area), formulated with 375U of

ISCOM as adjuvant (from Darrel J. Irvine, Howard Hughes Medical Institute) on weeks 0, 8, 24 and 40. Serum was collected before (pre-bleed) and two weeks after each immunization to monitor the antibody responses.

Design of C.1086 constructs and mutagenesis—All C.1086 proteins generated in the study correspond to 31–664 residues (HxB2 numbering) of C.1086 sequence (Genebank id FJ444392.1) and contain K160N (improve binding to PG9 bnAb), V295N (2G12 binding) and N334S (improve binding to PGT121 and 10–1074) mutations. C.1086 WT (508RRRRRR511 or 508R6511 to increase furin cleavage efficiency), SOSIP (A501C/T605C, 508RRRRRR511) (Sanders et al., 2013), NFL (Native Flexibly Linked, I559P, $^{508}(GGGGS)_2{}^{511}$) (Sharma et al., 2015), UFO (Uncleaved preFusion Optimized, $^{508}(GGGGS)_2{}^{511}$, ^{547}NPDWLPDM^{569}, no disulphide linkage A501C-T605C) (Kong et al., 2016), UFO-v2 ($^{508}(GGGGS)_2{}^{511}$, ^{547}NPDWLPDM^{569}, E64K/T316W/A433P) env inserts with GMCSF leader sequence (MWLQGLLLL GTVACSIS) were synthesized by GenScript and subcloned between ClaI and NheI sites of pGA1 vector (KanR). For generating V2 hotspot (HS) mutants, residues 166–173 in V2 hotspot region of C.1086 differing from the Clade C Consensus sequence i.e. positions 166,170,172 and 173 were mutated to either dominant and/or sub-dominant amino acids present in the consensus sequence. Mutagenesis was done by inverse PCR using non-overlapping forward and reverse primers. The mutant codon was present at the 5’ end of the forward primer(Jain and Varadarajan, 2014). pGA1 vector (KanR) expressing C.1086 UFO-v2 was used as the parent/template for V2-HS PCR reactions. NEB® 5-alpha E. coli cells (NEB, catalog no C2987H) and Sanger sequencing were used to transform, screen and confirm the positive clones respectively. Mutant pCDNA3.1 full length C.1086 K160N env bearing plasmids (used in neutralization mapping assays) were generated by introducing mutant codons as described above using pCDNA3.1 C.1086 K160N vector (AmpR) as template for PCR reactions and transformation of the blunt ligated mixture in NEB® Stable Competent *E. coli* cells (NEB, catalog no C3040H, 30°C). To generate gp70 C.1086 V1V2 RQ(H/Y)173 constructs, gp70 (design of gp70 V1V2 has been described previously (Zolla-Pazner et al., 2014)) was synthesized by Genescript in frame with C.1086 V1V2 (res. 120–204; K166R/H170Q for C.1086 V1V2 RQH^{173} and K166R/H170Q/H173Y for C.1086 V1V2 RQY^{173}) at its C terminus, and GMCSF leader sequence followed by 6xHis tag in-frame at its N terminus, and sub-cloned between ClaI and NheI sites in pGA1 vector. The BG505 SOSIP env insert (Genebank id ANG65466.1, res. 31–664, A501C/T605C/T332N, ^{508}RRRRRR^{511}, (Sanders et al., 2013)) was synthesized by Genescript with GMCSF leader sequence at its N terminus and sub-cloned between ClaI and NheI sites of pGA1 vector. To generate V2-HS mutants of BG505 SOSIP, we used inverse PCR using non-overlapping forward and reverse primers as described above for generating C.1086 V2-HS mutants.

Gp70_sequence:
^{N_terminus}VYNITWEVTNGDRETVWAISGNHPLWTWWPVLTPDLCMLALSGPPHWGL
EYQAPYSSPPGPPCCSGSSGSSAGCSRDCDEPLTSLTPRCNTAWNRLKLDQVTHKSSE
GFYVCPGSHRPREAKSCGGPDSFYCASWGCETTGRVYWKPSSSWDYITVDNNLTTS
QAVQVCKDNKWCNPLAIQFTNAGKQVTSWTTGHYWGLRLYVSGRDPGLTFGIRLR
YQNLGPRVPIGPNPVLADQLSLPRPNPLPKPAKSPP^{C_terminus}.

Purification of protein—The env gp140 glycoproteins cloned in KanR pGA1 plasmid were transiently expressed from Expi293F cells using the ExpifectamineTM 293 transfection kit (ThermoScientific) per manufacture's protocol and grown at 37°C, 8% CO_2 at 130rpm. The supernatant was harvested 72hrs after transfection in presence of EDTA free protease inhibitor (Millipore Sigma, catalog no 11836170001) and affinity purified by *Galanthus nivalis* lectin agarose (Vector Labs, catalog no AL-1243-5, pre-equilibrated with PBS). Bound protein was eluted in presence of 1M methyl α-D-mannopyranoside (Sigma). The protein was dialyzed against PBS and subjected to size-exclusion chromatography using a Superdex 200 Increase 10/300 GL (Sigma, GE Healthcare product) column on an AktaTM Pure (GE) system. The trimeric peak was collected, concentrated using Amicon Ultra-4, MWCO 100kDa, and quantified by BCA assay (Pierce™, ThermoScientific). To obtain highly monodisperse trimeric population for HDX-MS and DLS experiments, an additional hydrophobic Interaction chromatography (HIC) based purification (described by Verkerke, et al., 2016 was done on SEC purified protein samples prior to experiments. The proteins purified from SEC were dialyzed against a high salt buffer A (2M NH_4SO_4, 100mM NaH_2PO_4, 0.02% sodium azide; pH 7.4), bound to a pre-equilibrated (high-salt buffer A) Hitrap Phenyl HP column (Cytiva, catalog no 17519501), and eluted using a linear gradient (0–100%) of low salt buffer B (0.1M NaH_2P04, sodium azide 0.02%, pH 7.4) using an Akta™ Pure system (GE). The eluates containing trimeric peak of interest were pooled, dialyzed against PBS, concentrated and quantified. In all cases, the trimeric status and purity of the proteins were confirmed by BN-PAGE (NuPAGE™, 4–12% Bis-Tris Protein Gels, ThermoScientific). The gp70 V1V2 proteins were purified by His based affinity purification, using HisPur™ Ni-NTA resin (ThermoFisher, catalog no 88221), as described in the manufacturer's protocol. Briefly, the supernatant was diluted (1:1) in equilibration buffer (20mM sodium phosphate, 300mM sodium chloride, 10mM imidazole in PBS, pH 7.4) and bound to HisPur™ Ni-NTA column (pre-equilibrated with equilibration buffer). The column was washed with wash buffer (25mM imidazole in PBS; pH 7.4) to remove non-specific loosely bound proteins, followed by elution of the protein in presence of 250mM imidazole in PBS, pH 7.4. The eluted protein was dialyzed against PBS, concentrated using Amicon Ultra-4, MWCO 10kDa, and quantified by BCA assay. The purity of the protein was monitored by SDS-PAGE, and western blot. BG505 SOSIP T332N protein used as reference in mass spectrometry-based experiments was expressed from pPPI4 vector (kindly provided by Dr. John P. Moore, Cornell University, NY, USA) in 293F cells and purified as described above for C.1086 env gp140 constructs. For all assays using rabbit purified IgGs, IgG was purified from immunized rabbit serum using Pierce™ Protein A IgG Purification Kit (ThermoFisher, cat. No. 44667) and dialyzed against PBS, as per manufacturer's instructions. The protein was concentrated using Amicon Ultra-4, MWCO 30kDa, and quantified by BCA assay.

Negative stain electron microscopy (NS-EM)—Protein samples were diluted to 0.02 mg/ml, applied to a carbon coated Cu400 grid, and stained with 2% (w/v) uranyl formate for 30–60 s. Data were collected on an FEI Tecnai Spirit T12 transmission electron microscope operating at 120 keV and equipped with a Tietz TVIPS CMOS camera. A magnification of 52,000x was used, resulting in a physical pixel size at the specimen plane of 2.05 Å. Data was collected using the Leginon software package (Suloway et al., 2005), and

processing (particle picking and stack creation) was performed in Appion (Lander et al., 2009). Two-dimensional classifications were performed using MSA/MRA method described by (Ogura et al., 2003). Class averages were inspected manually and compared to previously published 2D class averages of HIV-1 Env SOSIP trimers (for example see (de Taeye et al., 2015)).

Enzyme-linked immunosorbent assay (ELISA) to screen V2 hotspot (HS) mutants for enhanced binding to V1V2 specific bnAbs—C.1086 V2 hotspot env mutant supernatants collected 48hrs after transient transfection of 293T cells were screened for increase in binding to PGT145 than the parent C.1086 UFO-v2. Env supernatants were immobilized onto ConA (Sigma, catalog no C2272, 25μg/ml in HEPES buffer i.e.,10mM HEPES, 151mM NaCl, 4.7mM KCl, 2mM CaCl2, 1.2mM MgCl2, 7.8mM Glucose, pH 8.5) coated ELISA maxisorp microtiter plates (ThermoFisher, catalog no 439454) at RT for 2hrs. The plates were blocked with 5% BSA + 4% Whey in PBS, RT, 1hr. Serially diluted env specific mAbs PGT145, PG9, PGT121, 3BNC117, 39F, CH58, CH59 Abs were added to the plates at RT, 1hr, after which plates were incubated with mouse anti-human biotin (BD Biosciences, catalog no 555785, 1:5000 dilution in 4% Whey buffer) and streptavidin horseradish peroxidase (Vector Labs, catalog no SA5004, 1:1000 dilution) as secondary and tertiary Abs respectively for 1hr at each step, RT. The plates were washed with PBS containing 0.05%Tween-20 (6 times) after each incubation step. The plates were developed with 3,3',5,5'- tetramethylbenzidine chromogenic substrate solution (KPL TMB Peroxidase substrate, SeraCare) in dark. The reactions were quenched with phosphoric acid. Equal concentrations of the env proteins (in supernatants) were added to the ELISA plates. The concentration was estimated by densitometric analyses of the env specific bands monitored by western blot of SDS-PAGE (+DTT) gel. ID6 (NIH AIDS reagents program, 0.5μg/ml), goat anti-mouse-HRP (SouthernBiotech, catalog no 1030–05, 1:40,000 dilution in 4% Whey buffer) were used as primary and secondary Abs for western blot. A450nm recorded from the developed ELISA plates were analyzed to measure binding area under the curve (AUC) against each mAb tested.

ELISA to estimate C.1086 specific responses in immunized serum—To monitor trimer specific responses, ELISA microtiter plates were coated with trimeric C.1086 UFO-v2-RQH^{173} protein at 2μg/ml (in PBS), overnight at 4°C. The plates were blocked with 5% BSA + 4% Whey in PBS, RT, 1hr. The plates were incubated with serially diluted serum at RT, 2hrs, followed by incubation with goat anti-rabbit HRP (SouthernBiotech, catalog no 4010–05, dilution 1:4000), RT, 1hr. The plates were washed with PBS containing 0.05%Tween-20 (6 times) after each incubation step and developed as described above. To monitor C.1086 V3 responses, ELISA plates coated overnight with V3 peptide (res. 297–330, 1μg/ml in PBS) were used. gp70 V1V2 specific responses were monitored by using plates coated with 2μg/ml His-tag purified gp70 C.1086 V1V2 RQH (K166R/H170Q/H173) and RQY (K166R/H170Q/H173Y) (Zolla-Pazner et al., 2014) proteins. A450nm recorded from the developed ELISA plates were analyzed to measure end-point titre associated with the serum responses.

Binding antibody multiplex assay (BAMA)—Binding antibody multiplex assay (BAMA) of the serum was performed as described previously (Tomaras et al., 2008; Zolla-Pazner et al., 2014). Briefly, serially diluted rabbit serum (5-fold dilution starting with 1:80) were tested for binding to color-coded beads by Bio-plex (Biorad). The beads were coated with avi tagged C.1086 WT, UFO-v2-RQH^{173}, UFO-v2-RQY^{173} gp140 and gp70 scaffolded proteins with V1V2 grafted from B.CaseA, 7060101641, CM244.ec1, TV1.21, 001428.2.42, CAP210.2.00.E8, C2101.c01, BJOX002000.03.2, BF1266_431a, 96ZM651.02, RHPA4259.7, Ce1086_B2, 62357.14, 700010058, 191084_B7, and TT31P.2F10.2792 HIV-1 strains. Biotinylated anti-rabbit IgG was used as secondary antibody followed by streptavidin conjugated fluorophore to monitor mean fluorescence intensity (MFI) signal at the dilutions tested. This was subsequently used to calculate binding area under curve (AUC) for analyses. Instances satisfying the following criteria were considered positive, i.e. (a)MFI at 1:80 dilution >100, (b) MFI at 1:80 > antigen specific cut-off (95th percentile of all pre-bleed for the study for each antigen), and (c) MFI > 3-fold that of the matched baseline or pre-bleed samples, both before and after blank bead subtraction.

Binding of purified serum IgGs to cell surface bound gp160 envs—293T cells were transfected with full-length env expressing plasmid using lipofectamine2000 (ThermoFisher, catalog no 11668027) as per the manufacturer's protocol. The cells were harvested 36 hours after transfection and incubated with 1μg/ml of purified rabbit IgG (week 42 i.e. two weeks after the final protein boost) for 45minutes, RT in presence of live/dead fixable stain (ThermoFisher, catalog no L34975). Env specific mAbs PGT145 (1μg/ml), PGT121 (0.5μg/ml), PG16 (1μg/ml) were used instead of rabbit IgG as controls to monitor expression of env on the cell surface. Goat anti-rabbit IgG PE (SouthernBiotech, cat. no. 4030–09, 1:1000 dilution) was used as secondary antibody, 30minutes, RT for monitoring binding to immunized rabbit IgG. To monitor binding to mAbs, mouse anti-human biotin (BD Biosciences, catalog no 555785, 1:5000 dilution) was used as secondary antibody followed by streptavidin conjugated PE (BD Biosciences, cat. no. 554061, 1:5000 dilution), 30min at RT each step. The cells were washed twice at 1500rpm, 5minutes, RT with BD FACS buffer after each incubation step. The samples were fixed in presence of 1% paraformaldehyde (in PBS) and acquired on LSRII flow cytometer. FlowJo v10.8.0 was used to analyse the data. pSV-A-MLV-env (NIH AIDS Reagent program) was used as negative control. Binding of purified rabbit IgG to this was used as reference to gate binding of corresponding rabbit IgG to live env positive cells. All env plasmids tested in the study constituting the global panel of HIV-1 envs were obtained from NIH AIDS Reagent program. Normalized frequency of env positive cells or normalized binding signal of serum (specific to rabbit R) to surface expressed full-length env x is plotted in heatmap shown in Figure 4F and is defined as $N_{R,x}$ = (Frequency of env$^+$ cells binding to serum, $F_{R,x}$ – Mean of the frequencies of env$^+$ cells binding to serum for all rabbits sampled, μ_x) divided by (standard deviation of the frequencies of env$^+$ cells binding to serum for all rabbits sampled, σ_x).

Bio-layer interferometry (BLI)—The assay was done in 384 well format on Octet Red384 platform, Pall ForteBio. Env specific mAbs (NIH-AIDS Reagent program) were

immobilized onto anti-human Fc coated biosensors at 5μg/ml. The purified protein was used as analyte (1000nM-12.5nM). Env-Antibody association (k_{on}) was monitored for 300s, followed by dissociation (k_{off}) for 600s. 10X Kinetics Buffer, Pall ForteBio was used as buffer for all steps in the assay. All steps were performed with agitation at 1000rpm. K_D (dissociation constant = k_{off}/k_{on}) was estimated by globally fitting the reference (buffer only) subtracted sensograms to a 1:1 binding model using ForteBio Octet Data Analysis v9 software. For time dependent affinity estimates, purified trimeric proteins C.1086 UFO-v2-RQH[173], UFO-v2-RQY[173] were serially diluted (800–12.5 nM) in 10X Kinetics Buffer, Pall ForteBio and incubated at room temperature (25°C) for 0, 4, 5, 8, 10, 12hrs, prior to affinity measurements by BLI. Residues targeted by various Env specific antibodies were mapped onto unliganded structure of BG505 SOSIP.DS trimer (pdb id 4ZMJ (Kwon et al., 2015)) using UCSF Chimera v1.14 (Pettersen et al., 2004).

For competition assays to monitor epitope specificity of the serum by BLI, IgG was purified from immunized rabbit serum. IgGs from pre-bleed and two weeks after the final protein boost were purified. To identify the epitope on C.1086 env protein targeted by rabbit purified IgG, we monitored competition between rabbit IgG and env specific mAb to bind the epitope in question; e.g. competition between purified rabbit IgG and HJ16to bind CD4 binding site on the protein. Anti-human Fc biosensor was immobilized with 5μg/ml of env specific mAb. Purified C.1086 UFO-v2-RQH173 (800nM) was pre-incubated with 6.4μM of purified rabbit IgG in 10X Kinetics Buffer, Pall ForteBio at 4°C, 1hr. This was used as analyte to monitor association with the immobilized biosensor for 300s and dissociation for 600s. (A) Protein only was used to estimate the maximum binding signal with desired mAb. (B) Protein + pre-bleed IgG served as negative control, while (C) signal from buffer + immunized purified IgG was used to monitor background or non-specific signal. (D) signal from protein + immunized purified rabbit IgG. % competition was calculated as 100*(D-C)/Mean(A, (B-C)). No non-specific interaction was observed between mAb immobilized biosensor and purified IgG alone. Area under the curve of the BLI sensogram (t=0 to 600s) was used as "signal" for analyses. Negative traces were inverted to calculate AUC. Competition >40% was considered positive based on examination of signals observed in (B), (D) and (C). Cases where $AUC_{Signal\ B} > 1.5 \times AUC_{Control\ signal\ C}$ were considered for analyses. All steps were performed with agitation at 1000rpm.

Neutralization assay—Neutralizing antibody activity in serum and purified IgG samples was measured in 96-well culture plates by using Tat-regulated luciferase (Luc) reporter gene expression to quantify reductions in virus infection in TZM-bl cells. TZM-bl cells were obtained from the NIH AIDS Research and Reference Reagent Program (catalog no 8129). Assays were performed with HIV-1 Env pseudotyped viruses produced in 293T cells essentially as previously described (Montefiori, 2009). Serum samples were heat-inactivated at 56°C for 45 minutes prior to assaying; purified IgG were not heat-inactivated prior to assaying. Samples were diluted over a range of 1:20 to 1:43,740 in cell culture medium and pre-incubated with virus (~150,000 relative light unit equivalents) for 1 hr at 37°C before addition of cells. Following a 48hr incubation, cells were lysed and Luc activity determined using a microtiter plate luminometer and BriteLite Plus Reagent (Perkin Elmer). Neutralization titers were the sample dilution at which relative luminescence units

(RLU) were reduced by 50% compared to RLU in virus control wells after subtraction of background RLU in cell control wells.

Antibody dependent cell mediated virus inhibition (ADCVI)—ADCVI assay was performed as previously described with some modifications (Kannanganat et al., 2016). Briefly, on day 1, CEM-NK^r cells were spinoculated at 1500×g for 3 hrs with tier2 Clade C SHIV1157ipd3N4 virus at 31 TCID50/mL. On day 2 of the assay, cryopreserved human donor PBMCs were thawed, washed, and counted. Cells were added to a V-bottom plate (Corning incorporated, Corning, NY) at a concentration of 1×10^5 cells/well and allowed to rest overnight. On day 3, purified rabbit IgG (250μg/ml) was incubated for 2 hrs with 1×10^4 infected CEM-NK^r cells that had been washed 3 times to remove unbound virus. After 2 hrs of incubation, purified rabbit IgG and infected CEM-NK^r cells were added to PBMCs. PGT121 (catalog no. ARP-12343; NIH AIDS Reagent Program) and EM4C04 (anti-influenza HA antibody) served as positive and negative controls respectively. Five days post incubation, cells were washed 2 times and fresh media was added to all wells. On day 7 post incubation, plates were spun at 1500 rpm for 5 mins and the supernatant was harvested and frozen until p27 Gap ELISAs could be performed.

SIV Gag p27 ELISA—High binding ELISA plates (Thermo Scientific, catalog no 44-2404-21) were coated at 0.5μg/mL with goat anti-mouse IgG2b (Southern Biotech, catalog no 1090–05) overnight at 4°C. Next day, plates were washed 6x with PBST (PBS + 0.05%Tween-20) and blocked with 1% BSA in PBST for 30 minutes at RT. Anti-p27 2F12 (NIH AIDS Reagent Program) antibody at 0.5 μg/mL was added to ELISA plates and incubated for 1 hr at 37°C. Plates were again washed 6x with PBST. Supernatant from ADCVI assays which were placed in the 4°C the night before, were treated with TritonX (Sigma) to a make a 0.5% Triton X solution to inactivate virus particles and release Gag. Gag supernatant was diluted 3-fold and added to ELISA plates and allowed to incubate for 1½ hr at 37°C. Plates were washed and biotinylated anti-SIV IgG diluted 1:1000 and added to each well. Plates were again incubated for 1 hr at 37°C. After 6x wash, neutralite-avidin peroxidase (N-HRP) (Southern Biotech) was diluted 1:4000 and added to each plate for 30 minutes at RT in the dark. After incubation, bound IgG was detected using tetramethylbenzidine substrate (KPL, Gaithersburg, MD). The reaction was stopped by adding 100 μl 2N H2SO4. The readings were recorded at 450nm.

Hydrogen/deuterium exchange mass spectrometry—5 μgs (52 pmol) per timepoint of each protein (1086.C UFO-v2-RQH^{173} and UFO-v2-RQY^{173} and BG505.664) were incubated in deuterated buffer (20mM PBS, 85% D2O, pH 7.5) for 3s, 1min, 30min, and 20hrs at room temperature. The reaction was stopped via diluting 1:1 in ice-cold quench buffer (200 mM tris(2-chlorethyl) phosphate (TCEP), 8 M urea, 0.2% formic acid) to a final pH of 2.5 and flash frozen in liquid nitrogen followed by storage in −80°C prior to analysis. Online pepsin digestion was performed and analyzed by LC-MS-IMS utilizing a Waters Synapt G2-Si Q-TOF mass spectrometer as described by (Verkerke et al., 2016) utilizing a 15 minute gradient. Pepsin digest eluates from un-deuterated sample LC-MS runs were collected, dried by speed vac, incubated in deuteration buffer for 1 hour at 85°C, and quenched as described above to prepare fully deuterated controls. Pepsin digest eluates from

undeuterated sample LC-MS runs were also collected, dried by speed vac, resuspended in mobile buffer for peptide identification using nano LC-MS on an Orbitrap Fusion mass spectrometer. A 2 cm trapping column and a 35 cm analytical column were freshly prepared in fused silica (100 μm ID) with 5 μM ReproSil-Pur C18 AQ beads (Dr. Maisch). 8 μL sample was injected and run using a 60-minute linear gradient from 2% to 30% acetonitrile in 0.1% FA, followed by 10 minutes of 80% acetonitrile. An EThcD method was optimized as follows: ion source 2.1 kV for positive mode; ion transfer tube temperature 350 °C; resolution: MS1 = 120000, MS2 = 30000; AGC target: MS1 = 2e5, MS2 = 1e5; and injection time: MS1 = 50 ms, MS2 = 60 ms. Orbitrap Fusion data was processed using Byonic (Version 3.8, Protein Metrics Inc.) to obtain a peptide reference list and identify peptic glycopeptides and glycosylation sites. Deuterium uptake analysis was performed with HD-Examiner (Sierra Analytics) followed by HX-Express v2 (Guttman et al., 2014; Weis et al., 2006). The percent exchange was normalized to the fully deuterated samples. Internal exchange standards (Pro-Pro-Pro-Ile [PPPI] and Pro-Pro-Pro-Phe [PPPF]) were included in each reaction to control for variations in ambient temperature during the labeling reactions.

Dynamic light scattering (DLS)—Dynamic light scattering (DLS) measurements were performed on a Dynapro Nanostar (Wyatt Technologies). Trimer samples were diluted to 1 mg/ml in PBS and centrifuged at 15,000×g for 20 min prior to loading of 10μl into a low-volume quartz cuvette. The mean estimated hydrodynamic radius, and polydispersity were generated from 30 acquisitions of 5 s at 20°C. For time dependent DLS experiments, the samples were diluted to 1 mg/mL in PBS and allowed to sit at room temperature (23°C) for 4 hours prior to centrifugation and measurement by DLS.

QUANTIFICATION AND STATISTICAL ANALYSES

All statistical analyses were performed using GraphPad Prism v8 software. All of the statistical details of experiments can be found in the figure legends of each figure, including the statistical tests used, value of n where n represents number of rabbits used for study (n=4 per immunization group), number of independent experiments carried out to represent the data, dispersion and precision measures (mean, median, SD). Data represent mean or mean ± SD as indicated in the figure legends. In some cases, data has been represented as box and whisker plots, where box extends from 25th to 75th percentile, median indicated by line, minimum and maximum values indicated by whiskers. intervals). Statistical significance between groups was performed by Mann-Whitney's U test and two-tailed Student's t test (small sample size, comparing time dependent mAb specific binding affinity parameters between C.1086 UFO-v2-RQ(H/Y)^{173} proteins). Two-Way ANNOVA test (Tukey's correction) for multiple comparisons. *p < 0.05, **p< 0.01, ***p<0.001, ****p<0.0001. p-values color coded by immunization group correspond to comparison with WT.

Supplementary Material

Refer to Web version on PubMed Central for supplementary material.

ACKNOWLEDGMENTS

We thank Dr. Lynn Morris for providing CAP228-16H mAbs, Dr. Jens Wrammert for anti-influenza EM4C04 Abs, Dr. Cynthia Derdeyn for the pCDNA3.1 C.1086 K160N plasmid, Dr. Pam Kozlowski for the biotinylated anti-SIV IgG protein, and Dr. John P. Moore for the pPPI4 BG505 SOSIP T332N plasmid. We also thank Dr. Genevieve Giny Fouda for providing PGT151, CAP256-VRC26.08, and PGDM1400 bnAbs. We thank Dr. Ruth Ruprecht and the HIV reagent resource for generously providing SHIV1157ipd3N4. We are extremely thankful to Dr. Du Yuhong, Emory University, GA, USA, for letting use the Octet RED384 instrument for the BLI experiments. We thank Dr. Raghavan Varadarajan, IISc, Bangalore 560012, India, and Dr. Robert Sonowal, Emory University, GA, USA, for their valuable suggestions. This work was supported in part by National Institutes of Health (NIH, United States) grants U19 AI109633 to R.R.A. and R01 AI140868 to K.K.L. and Office of research Infrastructure Programs (ORIP/NIH) base grant P51 OD011132 to YNPRC. Work related to negative-stain electron microscopy done at A.B.W.'s lab was supported by the Bill and Melinda Gates Foundation through the Collaboration for AIDS Vaccine Discovery (CAVD) grant OPP1115782 to A.B.W.

REFERENCES

Arunachalam PS, Charles TP, Joag V, Bollimpelli VS, Scott MKD, Wimmers F, Burton SL, Labranche CC, Petitdemange C, Gangadhara S, et al. (2020). T cell-inducing vaccine durably prevents mucosal SHIV infection even with lower neutralizing antibody titers. Nat. Med 26, 932–940. 10.1038/s41591-020-0858-8. [PubMed: 32393800]

Bale S, Martine A, Wilson R, Behrens AJ, Le Fourn V, de Val N, Sharma SK, Tran K, Torres JL, Girod PA, et al. (2018). Cleavage-independent HIV-1 trimers from CHO cell lines elicit robust autologous tier 2 neutralizing antibodies. Front. Immunol 9, 1116. 10.3389/fimmu.2018.01116. [PubMed: 29881382]

Barouch DH, Liu J, Li H, Maxfield LF, Abbink P, Lynch DM, Iampietro MJ, SanMiguel A, Seaman MS, Ferrari G, et al. (2012). Vaccine protection against acquisition of neutralization-resistant SIV challenges in rhesus monkeys. Nature 482, 89–93. 10.1038/nature10766. [PubMed: 22217938]

Bekker LG, Moodie Z, Grunenberg N, Laher F, Tomaras GD, Cohen KW, Allen M, Malahleha M, Mngadi K, Daniels B, et al. (2018). Subtype C ALVAC-HIV and bivalent subtype C gp120/MF59 HIV-1 vaccine in low-risk, HIV-uninfected, South African adults: a phase 1/2 trial. Lancet HIV 5, e366–e378. 10.1016/S2352-3018(18)30071-7. [PubMed: 29898870]

Bontempo A, Garcia MM, Rivera N, and Cayabyab MJ (2020).A systematic approach to HIV-1 vaccine immunogen selection. AIDS Res. Hum. Retrovir 36, 762–770. 10.1089/AID.2019.0239. [PubMed: 32056466]

Bricault CA, Yusim K, Seaman MS, Yoon H, Theiler J, Giorgi EE, Wagh K, Theiler M, Hraber P, Macke JP, et al. (2019). HIV-1 neutralizing antibody signatures and application to epitope-targeted vaccine design. Cell Host Microbe 25, 59–72 e58. 10.1016/j.chom.2018.12.001. [PubMed: 30629920]

Burton S, Spicer LM, Charles TP, Gangadhara S, Reddy PBJ, Styles TM, Velu V, Kasturi SP, Legere T, Hunter E, et al. (2019). Clade C HIV-1 envelope vaccination regimens differ in their ability to elicit antibodies with moderate neutralization breadth against genetically diverse tier 2 HIV-1 envelope variants. J. Virol 93, e01846–18. 10.1128/JVI.01846-18. [PubMed: 30651354]

Cimbro R, Gallant TR, Dolan MA, Guzzo C, Zhang P, Lin Y, Miao H, Van Ryk D, Arthos J, Gorshkova I, et al. (2014). Tyrosine sulfation in the second variable loop (V2) of HIV-1 gp120 stabilizes V2-V3 interaction and modulates neutralization sensitivity. Proc. Natl. Acad. Sci. USA 111, 3152–3157. 10.1073/pnas.1314718111. [PubMed: 24569807]

de Taeye SW, Ozorowski G, Torrents de la Pena A, Guttman M, Julien JP, van den Kerkhof TL, Burger JA, Pritchard LK, Pugach P, Yasmeen A, et al. (2015). Immunogenicity of stabilized HIV-1 envelope trimers with reduced exposure of non-neutralizing epitopes. Cell 163, 1702–1715. 10.1016/j.cell.2015.11.056. [PubMed: 26687358]

deCamp A, Hraber P, Bailer RT, Seaman MS, Ochsenbauer C, Kappes J, Gottardo R, Edlefsen P, Self S, Tang H, et al. (2014). Global panel of HIV-1 Env reference strains for standardized assessments of vaccine-elicited neutralizing antibodies. J. Virol 88, 2489–2507. 10.1128/JVI.02853-13. [PubMed: 24352443]

Doria-Rose NA, Schramm CA, Gorman J, Moore PL, Bhiman JN, DeKosky BJ, Ernandes MJ, Georgiev IS, Kim HJ, Pancera M, et al. (2014). Developmental pathway for potent V1V2-directed HIV-neutralizing antibodies. Nature 509, 55–62. 10.1038/nature13036. [PubMed: 24590074]

Dubrovskaya V, Guenaga J, de Val N, Wilson R, Feng Y, Movsesyan A, Karlsson Hedestam GB, Ward AB, and Wyatt RT (2017). Targeted N-glycan deletion at the receptor-binding site retains HIV Env NFL trimer integrity and accelerates the elicited antibody response. PLoS Pathog. 13, e1006614. 10.1371/journal.ppat.1006614. [PubMed: 28902916]

Dubrovskaya V, Tran K, Ozorowski G, Guenaga J, Wilson R, Bale S, Cottrell CA, Turner HL, Seabright G, O'Dell S, et al. (2019). Vaccination with glycan-modified HIV NFL envelope trimer-liposomes elicits broadly neutralizing antibodies to multiple sites of vulnerability. Immunity 51, 915–929 e917. 10.1016/j.immuni.2019.10.008. [PubMed: 31732167]

Escolano A, Gristick HB, Gautam R, DeLaitsch AT, Abernathy ME, Yang Z, Wang H, Hoffmann MAG, Nishimura Y, Wang Z, et al. (2021). Sequential immunization of macaques elicits heterologous neutralizing antibodies targeting the V3-glycan patch of HIV-1 Env. Sci. Transl. Med 13, eabk1533. 10.1126/scitranslmed.abk1533. [PubMed: 34818054]

Escolano A, Steichen JM, Dosenovic P, Kulp DW, Golijanin J, Sok D, Freund NT, Gitlin AD, Oliveira T, Araki T, et al. (2016). Sequential immunization elicits broadly neutralizing anti-HIV-1 antibodies in Ig knockin mice. Cell 166, 1445–1458 e1412. 10.1016/j.cell.2016.07.030. [PubMed: 27610569]

Excler JL, Ake J, Robb ML, Kim JH, and Plotkin SA (2014). Nonneutralizing functional antibodies: a new "old" paradigm for HIV vaccines. Clin. Vaccine Immunol 21, 1023–1036. 10.1128/CVI.00230-14. [PubMed: 24920599]

Falkowska E, Le KM, Ramos A, Doores KJ, Lee JH, Blattner C, Ramirez A, Derking R, van Gils MJ, Liang CH, et al. (2014). Broadly neutralizing HIV antibodies define a glycan-dependent epitope on the prefusion conformation of gp41 on cleaved envelope trimers. Immunity 40, 657–668. 10.1016/j.immuni.2014.04.009. [PubMed: 24768347]

Geretti AM, Harrison L, Green H, Sabin C, Hill T, Fearnhill E, Pillay D, and Dunn D; UK Collaborative Group on HIV Drug Resistance (2009). Effect of HIV-1 subtype on virologic and immunologic response to starting highly active antiretroviral therapy. Clin. Infect. Dis 48, 1296–1305. 10.1086/598502. [PubMed: 19331585]

Gorny MK, Pan R, Williams C, Wang XH, Volsky B, O'Neal T, Spurrier B, Sampson JM, Li L, Seaman MS, et al. (2012). Functional and immunochemical cross-reactivity of V2-specific monoclonal antibodies from HIV-1-infected individuals. Virology 427, 198–207. 10.1016/j.virol.2012.02.003. [PubMed: 22402248]

Gray GE, Bekker LG, Laher F, Malahleha M, Allen M, Moodie Z, Grunenberg N, Huang Y, Grove D, Prigmore B, et al. (2021). Vaccine efficacy of ALVAC-HIV and bivalent subtype C gp120-MF59 in adults. N. Engl. J. Med 384, 1089–1100. 10.1056/NEJMoa2031499. [PubMed: 33761206]

Gray GE, Huang Y, Grunenberg N, Laher F, Roux S, Andersen-Nissen E, De Rosa SC, Flach B, Randhawa AK, Jensen R, et al. (2019). Immune correlates of the Thai RV144 HIV vaccine regimen in South Africa. Sci. Transl. Med 11, eaax1880. 10.1126/scitranslmed.aax1880. [PubMed: 31534016]

Guenaga J, de Val N, Tran K, Feng Y, Satchwell K, Ward AB, and Wyatt RT (2015). Well-ordered trimeric HIV-1 subtype B and C soluble spike mimetics generated by negative selection display native-like properties. PLoS Pathog. 11, e1004570. 10.1371/journal.ppat.1004570. [PubMed: 25569572]

Guenaga J, Garces F, de Val N, Stanfield RL, Dubrovskaya V, Higgins B, Carrette B, Ward AB, Wilson IA, and Wyatt RT (2017). Glycine substitution at helix-to-coil transitions facilitates the structural determination of a stabilized subtype C HIV envelope glycoprotein. Immunity 46, 792–803 e793. 10.1016/j.immuni.2017.04.014. [PubMed: 28514686]

Guttman M, Garcia NK, Cupo A, Matsui T, Julien JP, Sanders RW, Wilson IA, Moore JP, and Lee KK (2014). CD4-induced activation in a soluble HIV-1 Env trimer. Structure 22, 974–984. 10.1016/j.str.2014.05.001. [PubMed: 24931470]

Guzzo C, Zhang P, Liu Q, Kwon AL, Uddin F, Wells AI, Schmeisser H, Cimbro R, Huang J, Doria-Rose N, et al. (2018). Structural constraints at the trimer apex stabilize the HIV-1 envelope in a

closed, antibody-protected conformation. mBio 9, e00955–18. 10.1128/mBio.00955-18. [PubMed: 30538178]

Haynes BF, Gilbert PB, McElrath MJ, Zolla-Pazner S, Tomaras GD, Alam SM, Evans DT, Montefiori DC, Karnasuta C, Sutthent R, et al. (2012). Immune-correlates analysis of an HIV-1 vaccine efficacy trial. N. Engl. J. Med 366, 1275–1286. 10.1056/NEJMoa1113425. [PubMed: 22475592]

He L, Kumar S, Allen JD, Huang D, Lin X, Mann CJ, Saye-Francisco KL, Copps J, Sarkar A, Blizard GS, et al. (2018). HIV-1 vaccine design through minimizing envelope metastability. Sci. Adv 4, eaau6769. 10.1126/sciadv.aau6769. [PubMed: 30474059]

Hessell AJ, Shapiro MB, Powell R, Malherbe DC, McBurney SP, Pandey S, Cheever T, Sutton WF, Kahl C, Park B, et al. (2018). Reduced cell-associated DNA and improved viral control in macaques following passive transfer of a single anti-V2 monoclonal antibody and repeated simian/human immunodeficiency virus challenges. J. Virol 92, e02198–17. 10.1128/JVI.02198-17. [PubMed: 29514914]

Huang D, Tran JT, Olson A, Vollbrecht T, Tenuta M, Guryleva MV, Fuller RP, Schiffner T, Abadejos JR, Couvrette L, et al. (2020). Vaccine elicitation of HIV broadly neutralizing antibodies from engineered B cells. Nat. Commun 11, 5850. 10.1038/s41467-020-19650-8. [PubMed: 33203876]

Jain PC, and Varadarajan R (2014). A rapid, efficient, and economical inverse polymerase chain reaction-based method for generating a site saturation mutant library. Anal. Biochem 449, 90–98. 10.1016/j.ab.2013.12.002. [PubMed: 24333246]

Jensen K, Nabi R, Van Rompay KKA, Robichaux S, Lifson JD, Piatak M Jr., Jacobs WR Jr., Fennelly G, Canfield D, Mollan KR, et al. (2016). Vaccine-elicited mucosal and systemic antibody responses are associated with reduced simian immunodeficiency viremia in infant rhesus macaques. J. Virol 90, 7285–7302. 10.1128/JVI.00481-16. [PubMed: 27252535]

Jones AT, Shen X, Walter KL, LaBranche CC, Wyatt LS, Tomaras GD, Montefiori DC, Moss B, Barouch DH, Clements JD, et al. (2019). HIV-1 vaccination by needle-free oral injection induces strong mucosal immunity and protects against SHIV challenge. Nat. Commun 10, 798. 10.1038/s41467-019-08739-4. [PubMed: 30778066]

Kannanganat S, Wyatt LS, Gangadhara S, Chamcha V, Chea LS, Kozlowski PA, LaBranche CC, Chennareddi L, Lawson B, Reddy PB, et al. (2016). High doses of GM-CSF inhibit antibody responses in rectal secretions and diminish modified vaccinia Ankara/simian immunodeficiency virus vaccine protection in TRIM5alpha-restrictive macaques. J. Immunol 197, 3586–3596. 10.4049/jimmunol.1600629. [PubMed: 27683750]

Kasturi SP, Kozlowski PA, Nakaya HI, Burger MC, Russo P, Pham M, Kovalenkov Y, Silveira EL, Havenar-Daughton C, Burton SL, et al. (2017). Adjuvanting a simian immunodeficiency virus vaccine with toll-like receptor ligands encapsulated in nanoparticles induces persistent antibody responses and enhanced protection in TRIM5alpha restrictive macaques. J. Virol 91, e01844–16. 10.1128/JVI.01844-16. [PubMed: 27928002]

Klasse PJ, Ketas TJ, Cottrell CA, Ozorowski G, Debnath G, Camara D, Francomano E, Pugach P, Ringe RP, LaBranche CC, et al. (2018). Epitopes for neutralizing antibodies induced by HIV-1 envelope glycoprotein BG505 SOSIP trimers in rabbits and macaques. PLoS Pathog. 14, e1006913. 10.1371/journal.ppat.1006913. [PubMed: 29474444]

Klasse PJ, LaBranche CC, Ketas TJ, Ozorowski G, Cupo A, Pugach P, Ringe RP, Golabek M, van Gils MJ, Guttman M, et al. (2016). Sequential and simultaneous immunization of rabbits with HIV-1 envelope glycoprotein SOSIP.664 trimers from clades A, B and C. PLoS Pathog. 12, e1005864. 10.1371/journal.ppat.1005864. [PubMed: 27627672]

Kong L, He L, de Val N, Vora N, Morris CD, Azadnia P, Sok D, Zhou B, Burton DR, Ward AB, et al. (2016). Uncleaved prefusion-optimized gp140 trimers derived from analysis of HIV-1 envelope metastability. Nat. Commun 7, 12040. 10.1038/ncomms12040. [PubMed: 27349805]

Kwon YD, Pancera M, Acharya P, Georgiev IS, Crooks ET, Gorman J, Joyce MG, Guttman M, Ma X, Narpala S, et al. (2015). Crystal structure, conformational fixation and entry-related interactions of mature ligand-free HIV-1 Env. Nat. Struct. Mol. Biol 22, 522–531. 10.1038/nsmb.3051. [PubMed: 26098315]

Lander GC, Stagg SM, Voss NR, Cheng A, Fellmann D, Pulokas J, Yoshioka C, Irving C, Mulder A, Lau PW, et al. (2009). Appion: an integrated, database-driven pipeline to facilitate EM image processing. J. Struct. Biol 166, 95–102. 10.1016/j.jsb.2009.01.002. [PubMed: 19263523]

Lee JH, Andrabi R, Su CY, Yasmeen A, Julien JP, Kong L, Wu NC, McBride R, Sok D, Pauthner M, et al. (2017). A broadly neutralizing antibody targets the dynamic HIV envelope trimer apex via a long, rigidified, and anionic beta-hairpin structure. Immunity 46, 690–702. 10.1016/j.immuni.2017.03.017. [PubMed: 28423342]

Liao HX, Bonsignori M, Alam SM, McLellan JS, Tomaras GD, Moody MA, Kozink DM, Hwang KK, Chen X, Tsao CY, et al. (2013). Vaccine induction of antibodies against a structurally heterogeneous site of immune pressure within HIV-1 envelope protein variable regions 1 and 2. Immunity 38, 176–186. 10.1016/j.immuni.2012.11.011. [PubMed: 23313589]

Liu Q, Acharya P, Dolan MA, Zhang P, Guzzo C, Lu J, Kwon A, Gururani D, Miao H, Bylund T, et al. (2017). Quaternary contact in the initial interaction of CD4 with the HIV-1 envelope trimer. Nat. Struct. Mol. Biol 24, 370–378. 10.1038/nsmb.3382. [PubMed: 28218750]

Lynch RM, Wong P, Tran L, O'Dell S, Nason MC, Li Y, Wu X, and Mascola JR (2015). HIV-1 fitness cost associated with escape from the VRC01 class of CD4 binding site neutralizing antibodies. J. Virol 89, 4201–4213. 10.1128/JVI.03608-14. [PubMed: 25631091]

McGuire AT (2019). Targeting broadly neutralizing antibody precursors: a naive approach to vaccine design. Curr. Opin. HIV AIDS 14, 294–301. 10.1097/COH.0000000000000548. [PubMed: 30946041]

Montefiori DC (2009). Measuring HIV neutralization in a luciferase reporter gene assay. Methods Mol. Biol 485, 395–405. 10.1007/978-1-59745-170-3_26. [PubMed: 19020839]

O'Donnell CD, Vogel L, Wright A, Das SR, Wrammert J, Li GM, McCausland M, Zheng NY, Yewdell JW, Ahmed R, et al. (2012). Antibody pressure by a human monoclonal antibody targeting the 2009 pandemic H1N1 virus hemagglutinin drives the emergence of a virus with increased virulence in mice. mBio 3, e00120–12. 10.1128/mBio.00120-12. [PubMed: 22647789]

Ogura T, Iwasaki K, and Sato C (2003). Topology representing network enables highly accurate classification of protein images taken by cryo electron-microscope without masking. J. Struct. Biol 143, 185–200. 10.1016/j.jsb.2003.08.005. [PubMed: 14572474]

Pancera M, Shahzad-Ul-Hussan S, Doria-Rose NA, McLellan JS, Bailer RT, Dai K, Loesgen S, Louder MK, Staupe RP, Yang Y, et al. (2013). Structural basis for diverse N-glycan recognition by HIV-1-neutralizing V1-V2-directed antibody PG16. Nat. Struct. Mol. Biol 20, 804–813. 10.1038/nsmb.2600. [PubMed: 23708607]

Pauthner M, Havenar-Daughton C, Sok D, Nkolola JP, Bastidas R, Boopathy AV, Carnathan DG, Chandrashekar A, Cirelli KM, Cottrell CA, et al. (2017). Elicitation of robust tier 2 neutralizing antibody responses in nonhuman primates by HIV envelope trimer immunization using optimized approaches. Immunity 46, 1073–1088 e1076. 10.1016/j.immuni.2017.05.007. [PubMed: 28636956]

Pejchal R, Walker LM, Stanfield RL, Phogat SK, Koff WC, Poignard P, Burton DR, and Wilson IA (2010). Structure and function of broadly reactive antibody PG16 reveal an H3 subdomain that mediates potent neutralization of HIV-1. Proc. Natl. Acad. Sci. U S A 107, 11483–11488. 10.1073/pnas.1004600107. [PubMed: 20534513]

Perez LG, Martinez DR, deCamp AC, Pinter A, Berman PW, Francis D, Sinangil F, Lee C, Greene K, Gao H, et al. (2017). V1V2-specific complement activating serum IgG as a correlate of reduced HIV-1 infection risk in RV144. PLoS One 12, e0180720. 10.1371/journal.pone.0180720. [PubMed: 28678869]

Pettersen EF, Goddard TD, Huang CC, Couch GS, Greenblatt DM, Meng EC, and Ferrin TE (2004). UCSF Chimera–a visualization system for exploratory research and analysis. J. Comput. Chem 25, 1605–1612. 10.1002/jcc.20084. [PubMed: 15264254]

Rademeyer C, Korber B, Seaman MS, Giorgi EE, Thebus R, Robles A, Sheward DJ, Wagh K, Garrity J, Carey BR, et al. (2016). Features of recently transmitted HIV-1 clade C viruses that impact antibody recognition: implications for active and passive immunization. PLoS Pathog. 12, e1005742. 10.1371/journal.ppat.1005742. [PubMed: 27434311]

Rerks-Ngarm S, Pitisuttithum P, Nitayaphan S, Kaewkungwal J, Chiu J, Paris R, Premsri N, Namwat C, de Souza M, Adams E, et al. (2009). Vaccination with ALVAC and AIDSVAX to prevent HIV-1 infection in Thailand. N. Engl. J. Med 361, 2209–2220. 10.1056/NEJMoa0908492. [PubMed: 19843557]

Rolland M, Edlefsen PT, Larsen BB, Tovanabutra S, Sanders-Buell E, Hertz T, deCamp AC, Carrico C, Menis S, Magaret CA, et al. (2012). Increased HIV-1 vaccine efficacy against viruses with genetic signatures in Env V2. Nature 490, 417–420. 10.1038/nature11519. [PubMed: 22960785]

Sanders RW, Derking R, Cupo A, Julien JP, Yasmeen A, de Val N, Kim HJ, Blattner C, de la Pena AT, Korzun J, et al. (2013). A next-generation cleaved, soluble HIV-1 Env trimer, BG505 SOSIP.664 gp140, expresses multiple epitopes for broadly neutralizing but not non-neutralizing antibodies. PLoS Pathog. 9, e1003618. 10.1371/journal.ppat.1003618. [PubMed: 24068931]

Sanders RW, and Moore JP (2017). Native-like Env trimmers as a platform for HIV-1 vaccine design. Immunol. Rev 275, 161–182. 10.1111/imr.12481. [PubMed: 28133806]

Sanders RW, van Gils MJ, Derking R, Sok D, Ketas TJ, Burger JA, Ozorowski G, Cupo A, Simonich C, Goo L, et al. (2015). HIV-1 VACCINES. HIV-1 neutralizing antibodies induced by native-like envelope trimers. Science 349, aac4223. 10.1126/science.aac4223. [PubMed: 26089353]

Sharma SK, de Val N, Bale S, Guenaga J, Tran K, Feng Y, Dubrovskaya V, Ward AB, and Wyatt RT (2015). Cleavage-independent HIV-1 Env trimers engineered as soluble native spike mimetics for vaccine design. Cell Rep. 11, 539–550. 10.1016/j.celrep.2015.03.047. [PubMed: 25892233]

Shen X, Laher F, Moodie Z, McMillan AS, Spreng RL, Gilbert PB, Huang Y, Yates NL, Grunenberg N, Juliana McElrath M, et al. (2020). HIV-1 vaccine sequences impact V1V2 antibody responses: a comparison of two Poxvirus Prime gp120 boost vaccine regimens. Sci. Rep 10, 2093. 10.1038/s41598-020-57491-z. [PubMed: 32034163]

Sok D, van Gils MJ, Pauthner M, Julien JP, Saye-Francisco KL, Hsueh J, Briney B, Lee JH, Le KM, Lee PS, et al. (2014). Recombinant HIV envelope trimer selects for quaternary-dependent antibodies targeting the trimer apex. Proc. Natl. Acad. Sci. U S A 111, 17624–17629. 10.1073/pnas.1415789111. [PubMed: 25422458]

Styles TM, Gangadhara S, Reddy PBJ, Hicks S, LaBranche CC, Montefiori DC, Derdeyn CA, Kozlowski PA, Velu V, and Amara RR (2019). Human immunodeficiency virus C.1086 envelope gp140 protein boosts following DNA/modified vaccinia virus Ankara vaccination fail to enhance heterologous anti-V1V2 antibody response and protection against clade C simian-human immunodeficiency virus challenge. J. Virol 93, e00934–19. 10.1128/JVI.00934-19. [PubMed: 31341049]

Suloway C, Pulokas J, Fellmann D, Cheng A, Guerra F, Quispe J, Stagg S, Potter CS, and Carragher B (2005). Automated molecular microscopy: the new Leginon system. J. Struct. Biol 151, 41–60. 10.1016/j.jsb.2005.03.010. [PubMed: 15890530]

Tassaneetrithep B, Tivon D, Swetnam J, Karasavvas N, Michael NL, Kim JH, Marovich M, and Cardozo T (2014). Cryptic determinant of alpha4beta7 binding in the V2 loop of HIV-1 gp120. PLoS One 9, e108446. 10.1371/journal.pone.0108446. [PubMed: 25265384]

Tomaras GD, Yates NL, Liu P, Qin L, Fouda GG, Chavez LL, Decamp AC, Parks RJ, Ashley VC, Lucas JT, et al. (2008). Initial B-cell responses to transmitted human immunodeficiency virus type 1: virion-binding immunoglobulin M (IgM) and IgG antibodies followed by plasma anti-gp41 antibodies with ineffective control of initial viremia. J. Virol 82, 12449–12463. 10.1128/JVI.01708-08. [PubMed: 18842730]

Torrents de la Pena A, Julien JP, de Taeye SW, Garces F, Guttman M, Ozorowski G, Pritchard LK, Behrens AJ, Go EP, Burger JA, et al. (2017). Improving the immunogenicity of native-like HIV-1 envelope trimers by hyperstabilization. Cell Rep. 20, 1805–1817. 10.1016/j.celrep.2017.07.077. [PubMed: 28834745]

Vaccari M, Gordon SN, Fourati S, Schifanella L, Liyanage NP, Cameron M, Keele BF, Shen X, Tomaras GD, Billings E, et al. (2016). Adjuvant-dependent innate and adaptive immune signatures of risk of SIVmac251 acquisition. Nat. Med 22, 762–770. 10.1038/nm.4105. [PubMed: 27239761]

van Eeden C, Wibmer CK, Scheepers C, Richardson SI, Nonyane M, Lambson B, Mkhize NN, Vijayakumar B, Sheng Z, Stanfield-Oakley S, et al. (2018). V2-Directed vaccine-like antibodies from HIV-1 infection identify an additional K169-binding light chain motif with broad ADCC activity. Cell Rep 25, 3123–3135 e3126. 10.1016/j.celrep.2018.11.058. [PubMed: 30540944]

Verkerke HP, Williams JA, Guttman M, Simonich CA, Liang Y, Filipavicius M, Hu SL, Overbaugh J, and Lee KK (2016). Epitope-independent purification of native-like envelope trimers from diverse HIV-1 isolates. J. Virol 90, 9471–9482. 10.1128/JVI.01351-16. [PubMed: 27512064]

Voss JE, Andrabi R, McCoy LE, de Val N, Fuller RP, Messmer T, Su CY, Sok D, Khan SN, Garces F, et al. (2017). Elicitation of neutralizing antibodies targeting the V2 apex of the HIV envelope trimer in a wild-type Animal model. Cell Rep. 21, 222–235. 10.1016/j.celrep.2017.09.024. [PubMed: 28978475]

Weis DD, Wales TE, Engen JR, Hotchko M, and Ten Eyck LF (2006). Identification and characterization of EX1 kinetics in H/D exchange mass spectrometry by peak width analysis. J. Am. Soc. Mass Spectrom 17, 1498–1509. 10.1016/j.jasms.2006.05.014. [PubMed: 16875839]

Xu K, Acharya P, Kong R, Cheng C, Chuang GY, Liu K, Louder MK, O'Dell S, Rawi R, Sastry M, et al. (2018). Epitope-based vaccine design yields fusion peptide-directed antibodies that neutralize diverse strains of HIV-1. Nat. Med 24, 857–867. 10.1038/s41591-018-0042-6. [PubMed: 29867235]

Yates NL, Liao HX, Fong Y, deCamp A, Vandergrift NA, Williams WT, Alam SM, Ferrari G, Yang ZY, Seaton KE, et al. (2014). Vaccine-induced Env V1-V2 IgG3 correlates with lower HIV-1 infection risk and declines soon after vaccination. Sci. Transl. Med 6, 228ra239. 10.1126/scitranslmed.3007730.

Yu Q, Wang B, Chen Z, Urabe G, Glover MS, Shi X, Guo LW, Kent KC, and Li L (2017). Electron-transfer/higher-energy collision dissociation (EThcD)-Enabled intact glycopeptide/glycoproteome characterization. J. Am. Soc. Mass Spectrom 28, 1751–1764. 10.1007/s13361-017-1701-4. [PubMed: 28695533]

Zolla-Pazner S, Alvarez R, Kong XP, and Weiss S (2019). Vaccine-induced V1V2-specific antibodies control and or protect against infection with HIV, SIV and SHIV. Curr. Opin. HIV AIDS 14, 309–317. 10.1097/COH.0000000000000551. [PubMed: 30994501]

Zolla-Pazner S, deCamp A, Gilbert PB, Williams C, Yates NL, Williams WT, Howington R, Fong Y, Morris DE, Soderberg KA, et al. (2014). Vaccine-induced IgG antibodies to V1V2 regions of multiple HIV-1 subtypes correlate with decreased risk of HIV-1 infection. PLoS One 9, e87572. 10.1371/journal.pone.0087572. [PubMed: 24504509]

Zolla-Pazner S, deCamp AC, Cardozo T, Karasavvas N, Gottardo R, Williams C, Morris DE, Tomaras G, Rao M, Billings E, et al. (2013). Analysis of V2 antibody responses induced in vaccinees in the ALVAC/AIDSVAX HIV-1 vaccine efficacy trial. PLoS One 8, e53629. 10.1371/journal.pone.0053629. [PubMed: 23349725]

Highlights

- The UFO design of C.1086 clade C envelope yields higher trimeric fraction
- Sequence-guided mutations at V2 hotspot region improve antigenicity of the V2 apex
- Optimized envelope trimers induce autologous neutralizing antibodies
- 173Y modification enhances breadth of V1V2-scaffold-specific antibodies

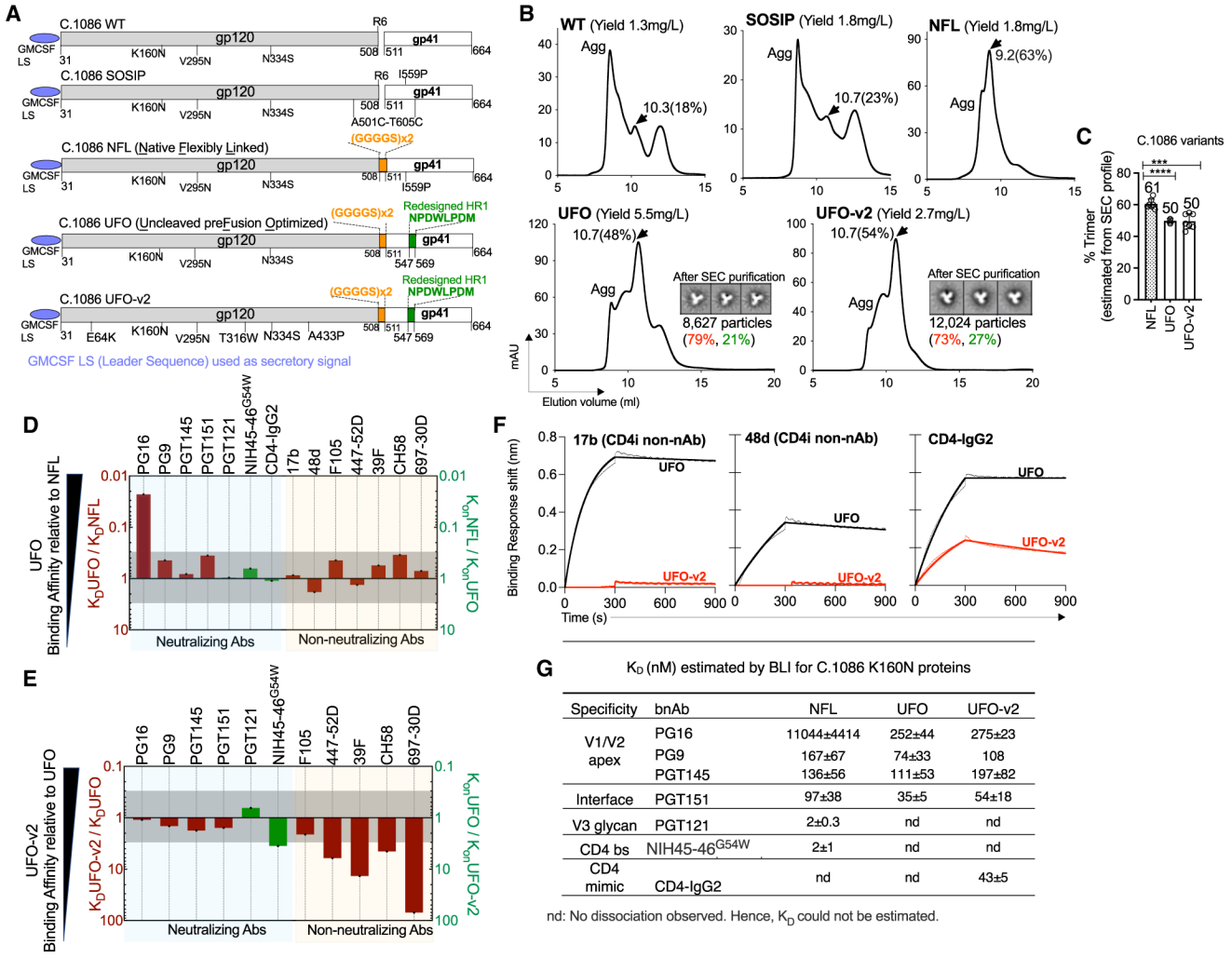

Specificity	bnAb	NFL	UFO	UFO-v2
V1/V2 apex	PG16	11044±4414	252±44	275±23
	PG9	167±67	74±33	108
	PGT145	136±56	111±53	197±82
Interface	PGT151	97±38	35±5	54±18
V3 glycan	PGT121	2±0.3	nd	nd
CD4 bs	NIH45-46^{G54W}	2±1	nd	nd
CD4 mimic	CD4-IgG2	nd	nd	43±5

nd: No dissociation observed. Hence, K_D could not be estimated.

Figure 1. Biophysical characterization of C.1086 base constructs

(A) Schematic representation of different C.1086 base constructs tested in the study.

(B) SEC profiles of 293F-expressed, GNL affinity-purified C.1086 base constructs. Trimeric peak (black arrow) elution volume and proportion (percentage, area under the curve [AUC]). Agg, aggregate/oligomeric peak. 2D class averages of the UFO and UFO-v2 trimers monitored by negative-stain electron microscopy shown at the bottom right of corresponding traces with total particles imaged (%native-like and %non-native like malformed trimers).

(C) Trimeric proportion of C.1086 variants (mean [value indicated on top of bar] ± SD [error bars]) of at least three independent transfection/purifications estimated from SEC profiles. Student's t test (two-tailed) for statistical comparisons, *p < 0.05, **p < 0.01, ***p < 0.001, ****p < 0.000.

(D) Comparison of binding affinities of UFO and NFL trimers for various env-specific mAbs. For instances where the K_D could not be calculated due to no observable dissociation in the experimental setting, K_{on} was used for comparison. A fold change in affinity within 3-fold range is shaded gray and not considered a significant change.

(E) Similar plot as described in (C) but comparing UFO-v2 versus UFO.

(F) Bio-layer interferometry (BLI) responses of 200 nM C.1086 UFO, UFO-v2 designs to CD4i non-nAbs, and CD4-IgG2.

(G) K_D (nM) of C.1086 variants against various bnAbs. Mean (at least two independent experiments) ± SD.

(D–G) All binding affinities estimated by BLI. All C.1086 constructs carried K160N/V295N/N334S changes.

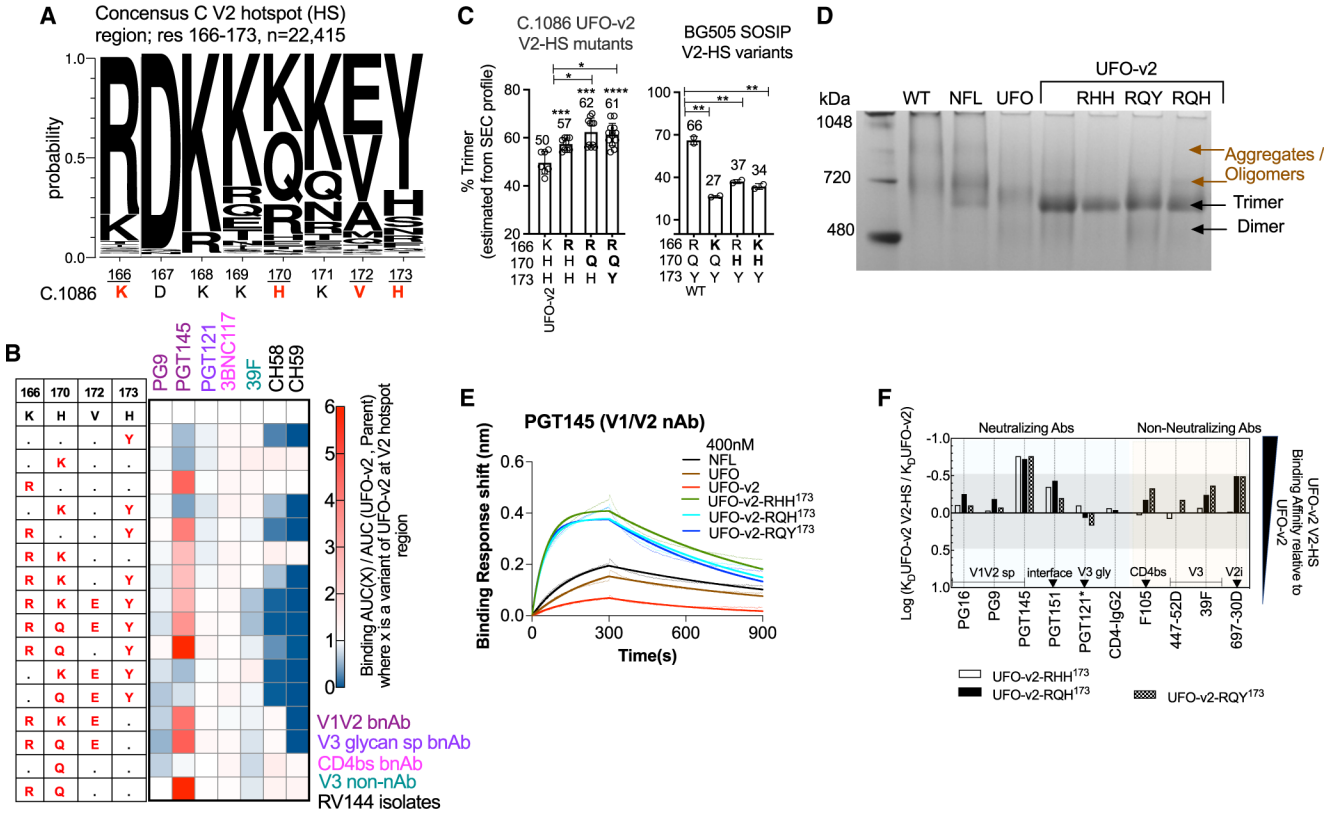

Figure 2. Sequence-guided mutations at the V2 hotspot region improve properties of well-formed trimmers

(A) V2 hotspot (V2-HS) region (res. 166–173) of clade C consensus sequence (n = 22,415) with corresponding C.1086 region mentioned below. C.1086 residues differing from the consensus sequence are in red.

(B) Influence of indicated V2-HS modifications in C.1086 UFO-v2 protein on binding to various mAbs, monitored by ELISA. The data are the average of more than two independent experiments.

(C) Trimeric proportion of C.1086 UFO-v2 (left) and BG505 SOSIP.664 V2-HS (right) variants; mean (value indicated) ± SD (error bars) estimated from SEC profiles of at least two independent purifications. *p < 0.05; **p < 0.01; ***p < 0.001; ****p < 0.0001 (Student's t test, two-tailed), (left) p value indicated on top of bar denotes comparison with UFO-v2, which has 166K,170H,173H.

(D) Blue native PAGE (BN-PAGE) of purified C.1086 proteins with molecular weight standard.

(E) BLI responses of different C.1086-purified designs (400 nM each) against V1/V2 trimer apex-specific PGT145 bnAbs.

(F) Comparison between binding affinities of optimized UFO-v2 V2-HS mutants relative to UFO-v2 against various env-specific mAbs. *KonUFO-v2/Kon UFO-v2 V2-HS for PGT121, as K_D could not be calculated due to no observable dissociation. A fold change in affinity within 3-fold range is shaded gray and not considered a significant change.

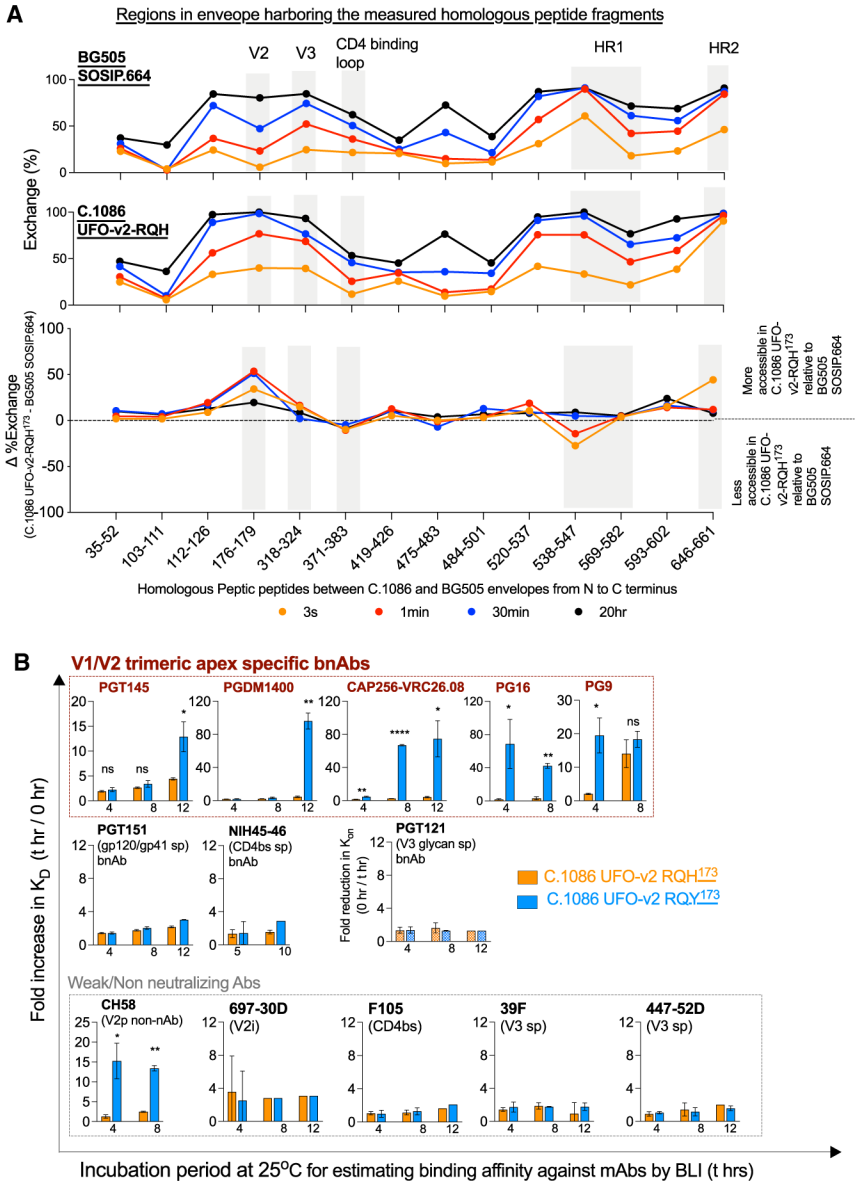

Figure 3. Structural properties of C.1086 UFO-v2-RQ(H/Y)^{173} trimers measured by HDX-MS and time-dependent BLI experiments

(A) Top: butterfly plots of BG505 SOSIP.664 and C.1086 UFO-v2-RQH^{173} proteins showing the percentage of exchange or the deuterium uptake for homologous peptide segments (indicated from N to C terminus) of the trimers detected in the experiment at each time point. Bottom: differences in percentage of exchange or deuterium uptake of homologous peptide segments of C.1086 UFO-v2-RQH^{173} relative to the BG505 SOSIP.664 trimer.

(B) Time-dependent fold reduction in binding affinity (K_D t hr/K_D 0 h) of C.1086 UFO-v2-RQH^{173} and UFO-v2-RQY^{173} immunogens against various env-specific mAbs measured by BLI at 25°C. In case of PGT121, fold reduction in association rate (K_{on} 0 h/K_{on} t hr) was plotted, as K_D could not be calculated due to no observable dissociation. Bars show mean,

error bars SD of at least three independent experiments. Student's t test (two-tailed) for statistical comparisons, *p < 0.05, **p < 0.01, ***p<0.001,****p<0.0001.

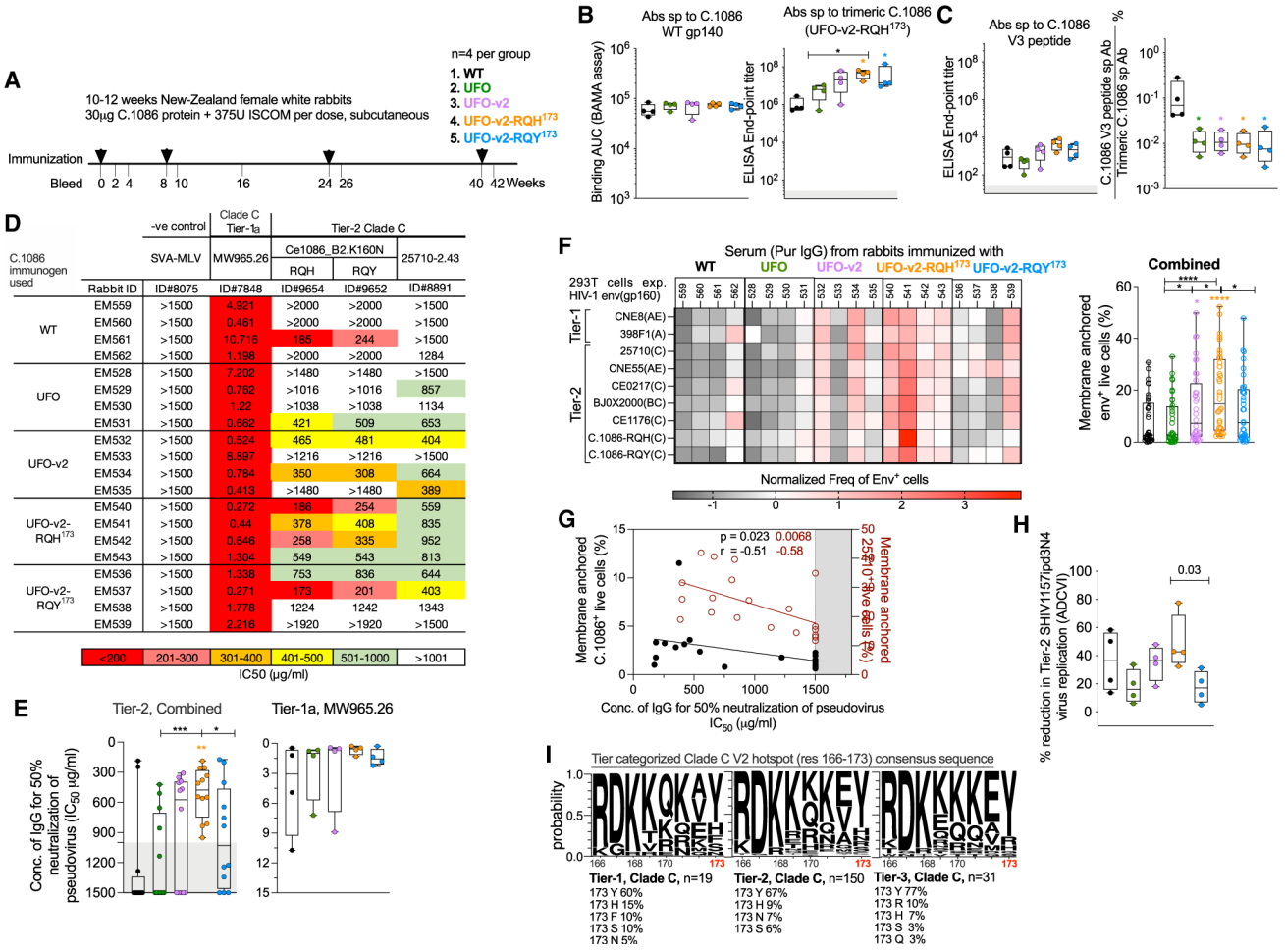

Figure 4. 166R and 170Q modifications in V2-HS of UFO-v2 (UFO-v2-RQH^{173}) enhance induction of moderate anti-viral antibody responses and binding to membrane-anchored tier2 envs

(A–C) Schematic overview of the immunogenicity regimen tested in rabbits (n = 4 per immunization group). Serum binding antibody responses against (B) C.1086 WT and trimeric UFO-v2-RQH^{173} proteins measured by binding antibody-mediated multiplex assay (BAMA; indicated by area under the curve [AUC]) and ELISA, respectively and (C) the V3 peptide (left) and normalized to total trimer-specific responses (right).

(D and E) Neutralizing antibody titer against tier1 and tier2 HIV-1 envs. See Table S3 for responses against other tier2 envs, which were mostly negligible. The concentration of purified IgG required to achieve 50% neutralization (IC_{50} μg/mL) is shown. In (E) IC_{50} >1,480 assigned 1,500 for ease of visualization in the graph.

(F) Binding of purified IgG (1 μg/mL) from immunized rabbits to broad multi-clade HIV-1 full-length envs expressed on transiently transfected 293T cells. See Figure S6D for representative flow plot and gating of env$^+$ live cells. Normalized frequency of env$^+$ live cells is plotted (see STAR Methods). Combined plot and env$^+$ frequencies measured against each env in the panel for each rabbit.

(G) Spearman's correlation between binding responses to membrane-anchored envs (C.1086 and 25710), and concentration of IgG required for 50% neutralization of the corresponding env-specific pseudovirus.

(H) Percentage of reduction in replication of clade C tier2 SHIV1157ipd3N4 virus in human peripheral blood mononuclear cells (PBMCs) by purified IgGs (250 μg/mL) from various immunized groups (percentage of ADCVI activity). Each data point represents the averaged data for a rabbit IgG from three independent experiments, each done in duplicate.

(B–H) All analyses correspond to serum collected 2 weeks post final protein boost. Refer to (A) for color coding of the immunization groups.

(I) V2-HS region of various tier-categorized consensus clade C sequences (Rademeyer et al., 2016).

(B, E, F, and H) Box and whisker plots where box extends from 25th to 75th percentile, median indicated by line, and minimum and maximum values indicated by whiskers. Statistical comparisons between groups by Mann-Whitney test (*$p < 0.05$, **$p < 0.01$, ***$p < 0.001$, ****$p < 0.0001$, p values color coded by group correspond to comparison with WT). All values plotted are the average of at least two independent experiments.

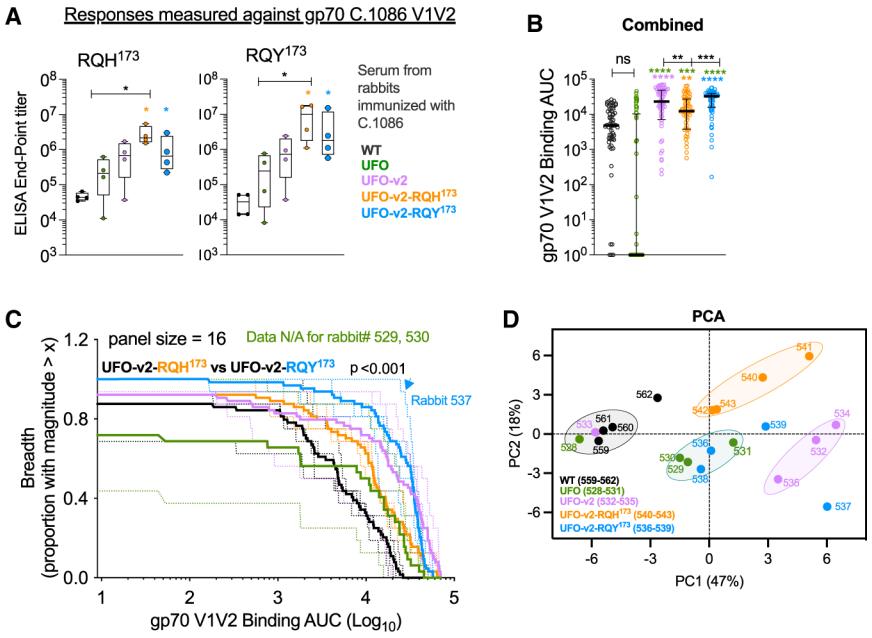

Figure 5. 173Y modification in UFO-v2-RQH^{173} enhances the breadth of V1V2-scaffold-specific responses

(A) Serum binding antibody responses of the immunized groups against gp70 C.1086 RQ(H/Y)^{173} V1V2 proteins. Plotted values are the average of two independent experiments.

(B) BAMA analyses (binding the AUC) of serially diluted immunized serum to V1V2 scaffolds from 16 cross-clade HIV-1 isolates (see Figure S6G). The combined plot uses the AUC values obtained against the panel for each rabbit.

(C) V1V2 breadth magnitude curves of all immunized rabbits (dotted line) with mean response of a group (bold line). Refer to (A) for color coding of the immunization groups. Unpaired two-tailed Kolmogorov-Smirnov test was used to see statistical difference between UFO-v2-RQH^{173} and UFO-v2-RQY^{173} groups.

(D) Principal component analyses (PCAs; using R) of serum characterization data obtained for all immunized rabbits. All analyses correspond to serum collected 2 weeks post final protein boost. Mann-Whitney test for statistical comparisons between groups was used. *p < 0.05, **p < 0.01, ***p < 0.001, ****p < 0.0001. p values color coded by group correspond to a comparison with the WT group, and in (B), those colored green correspond to a comparison with the UFO group.

(A and B) Box and whisker plots where box extends from 25th to 75th percentile, median indicated by line, and minimum and maximum values indicated by whiskers.

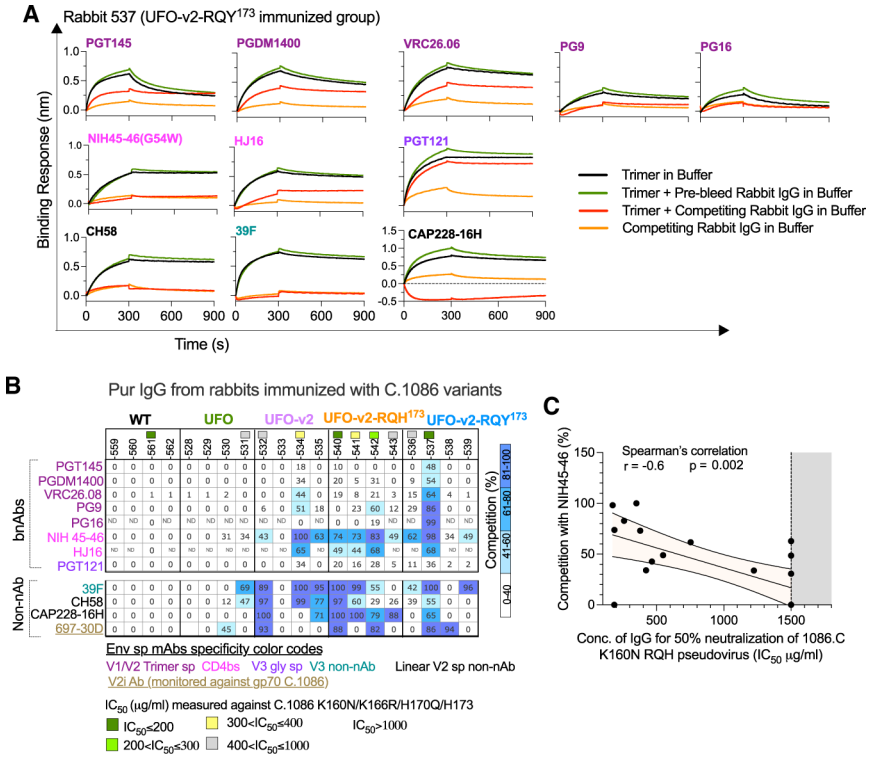

Figure 6. Mapping binding specificity of Abs elicited in rabbits immunized with C.1086 variants

(A) Representative BLI traces of competition binding experiment for purified IgG (rabbit #537) against env-specific mAbs.

(B) Heatmap showing percentage of competition of rabbit-purified IgGs with env-specific mAbs to bind to C.1086 UFO-v2-RQH^{173} trimers and gp70 C.1086 V1V2 in the case of 697-30D V2i mAbs.

(A and B) Purified IgGs from 2 weeks after final protein boost used for analyses. Values <40%, false positive. Not determined (ND) due to <1.5-fold difference in signals between background (buffer + purified IgG) and positive (buffer + trimer) control binding signals for the mAbs. C.1086 K160N RQH^{173} neutralization IC_{50} values (concentration of IgG required for 50% neutralization of the virus) of rabbit-purified IgG (filled squares color coded based on IC_{50} values; see Figure 4D) are mentioned above the rabbit codes. Data are representative of at least three independent experiments.

(C) Spearman's correlation (two-tailed) between C.1086 K160N RQH^{173} neutralization IC_{50} and competition (%) with NIH45-46 (estimated in B). Shaded orange area represents 95% confidence band. IC_{50} >1,480 assigned 1,500 for ease of visualization in the graph (shaded gray area).

KEY RESOURCES TABLE

REAGENT or RESOURCE	SOURCE	IDENTIFIER
Antibodies		
PGT145	NIH AIDS Reagent Program	Cat# ARP-12703; RRID: AB_2491054
PGT151	Laboratory of Dr. Genevieve Giny Fouda, Duke University (Falkowska et al., 2014)	N/A
PG9	NIH AIDS Reagent Program	Cat# ARP-12149; RRID: AB_2491030
PG16	NIH AIDS Reagent Program	Cat# ARP-12150; RRID: AB_2491031
PGT121	NIH AIDS Reagent Program	Cat# ARP-12343; RRID: AB_2491041
447-52D	NIH AIDS Reagent Program	Cat# ARP-4030; RRID: AB_2491016
48d	NIH AIDS Reagent Program	Cat# ARP-1756; RRID: AB_2905601
39f	NIH AIDS Reagent Program	Cat# ARP-11437; RRID: AB_2905602
17b	NIH AIDS Reagent Program	Cat# ARP-4091; RRID: AB_2905603
CAP256-VRC26.08	Laboratory of Dr. Genevieve Giny Fouda, Duke University (Doria-Rose et al., 2014)	N/A
NIH45-46^{G54W}	NIH AIDS Reagent Program	Cat# ARP-12174; RRID: AB_2491035
3BNC117		Cat# ARP-12474; RRID: AB_2491033
CD4-IgG2	NIH AIDS Reagent Program	Cat# 11780; RRID: AB_2905604
PGDM1400	Laboratory of Dr. Genevieve Giny Fouda, Duke University (Sok et al., 2014)	N/A
CAP228-16H	Laboratory of Dr. Lynn Morris, Wits University (van Eeden et al., 2018)	N/A
697-30D	NIH AIDS Reagent Program	Cat# ARP-7371; RRID: AB_2905605
ID6	NIH AIDS Reagent Program	Cat# ARP-2343; RRID: AB_2905606
Mouse Anti-human biotin	BD Biosciences	Cat# 555785; RRID: AB_396120
Goat anti-mouse-HRP	Southern Biotech	Cat#1030-05; RRID: AB_2619742
Goat anti-rabbit HRP	Southern Biotech	Cat# 4010-05; RRID: AB_2632593
Streptavidin HRP	Vector Labs	Cat#SA5004; RRID: AB_2336509
Goat anti-rabbit IgG PE	Southern Biotech	Cat#4030-09; RRID: AB_2795937
Anti-p27 2F12	NIH AIDS Reagent Program	Cat# ARP-1610; RRID: AB_2905607
Goat anti-mouse IgG2b	Southern Biotech	Cat# 1090-05; RRID: AB_2794521
Biotinylated Anti-SIV IgG	Laboratory of Dr Pam Kozlowski, LSUHSC School of Medicine (Jensen et al., 2016)	N/A
EM4C04 Anti-Influenza Ab	Laboratory of Dr. Jens Wrammert, Emory University (O'Donnell et al., 2012)	N/A
Bacterial and viral strains		
Bacteria: NEB® 5-alpha Competent E. coli (High Efficiency)	NEB	Cat# C2987H
Bacteria: NEB® Stable Competent E. coli cells	NEB	Cat# C3040H

REAGENT or RESOURCE	SOURCE	IDENTIFIER
Tier2 Clade C SHIV1157ipd3N4 virus	Laboratory of Dr. Ruth Ruprecht and the HIV reagent resource	Cat# ARP-11689
Biological Samples		
Serum samples from Rabbits	This Manuscript	N/A
Human PBMCs	This Manuscript	N/A
Chemicals, peptides, and recombinant proteins		
C.1086 NFL (with I559P)	Guenaga et al., 2017	N/A
C.1086 SOSIP	This Manuscript	N/A
C.1086 UFO (no disulphide linkage between A501 and T605)	He et al., 2018	N/A
C.1086 UFO-v2	This Manuscript	N/A
C.1086 UFO-v2-RHH^{173}	This Manuscript	N/A
C.1086 UFO-v2-RQH^{173}	This Manuscript	N/A
C.1086 UFO-v2-RQY^{173}	This Manuscript	N/A
C.1086 UFO-v2-V2-HS mutants	This Manuscript	N/A
C.1086 UFO-v2-RQH^{173} Avi	This Manuscript	N/A
C.1086 UFO-v2-RQY^{173} Avi	This Manuscript	N/A
BG505 SOSIP.664 WT	Sanders et al., 2013	N/A
BG505 SOSIP.664 KQY	This Manuscript	N/A
BG505 SOSIP.664 RHY	This Manuscript	N/A
BG505 SOSIP.664 KHY	This Manuscript	N/A
gp70 C.1086 RQH^{173} V1V2	This Manuscript	N/A
gp70 C.1086 RQY^{173} V1V2	This Manuscript	N/A
gp70 V1V2 global panel	Zolla-Pazner et al., 2014	N/A
C.1086 V3 peptide ^{N}TRPNNNT RKSIRIGPGQTFYA TGDIIGNIRQAH^{C}	This Manuscript	N/A
Phusion High-Fidelity PCR Master Mix with HF Buffer	ThermoScientific	Cat# F531S
T4 DNA Ligase	NEB	Cat# M0202S
T4 Polynucleotide Kinase	NEB	Cat# M0201S
DpnI	NEB	Cat# R0176S
NheI-HF	NEB	Cat# R3131S
ClaI	NEB	Cat# R0197S
Galanthus nivalis lectin-agarose	Vector Laboratories	Cat# AL-1243-5
Expifectamine™ 293 transfection kit	ThermoScientific	Cat# A14524
Expi293™ Expression Medium	ThermoScientific	Cat# A1435101
cOmplete™, Mini Protease Inhibitor Cocktail	Millipore Sigma	Cat# 11836153001
Methyl α-D-mannopyranoside	Millipore Sigma	Cat# M6882-25G
Superdex 200 Increase 10/300 GL	Cytiva (GE Healthcare LifeSciences)	Cat# GE28-9909-44
Amicon Ultra-4, MWCO 100kDa	Millipore Sigma	Cat# UFC910024
Pierce™ Protein A IgG Purification Kit, 1 mL	ThermoScientific	Cat# 44667

REAGENT or RESOURCE	SOURCE	IDENTIFIER
NuPAGE™, 4-12% Bis-Tris Protein Gels	ThermoScientific	Cat# NP0321BOX
NativeMark™ Unstained Protein Standard	ThermoScientific	Cat# LC0725
DMEM (Dulbecco's Modified Eagle's Medium)	Corning	Cat# 10-013-CV
HyClone™ Fetal Bovine Serum (FBS)	Cytiva (GE Healthcare LifeSciences)	Cat# SH30910.03
10X Kinetics Buffer	Pall ForteBio	Cat# 18-5032
Slide-A-Lyzer™ Dialysis Cassettes, 20K MWCO, 30 mL	ThermoScientific	Cat# 66030
Lipofectamine™ 2000 Transfection Reagent	Thermo Scientific	Cat# 11668019
Amicon® Ultra-15 Centrifugal Filter Unit, 30KDa, 24	Millipore	Cat# UFC903024
Precision Plus Protein™ Kaleidoscope™ Prestained Protein Standards	BioRad	Cat# 1610375
Microplate, 384 well, PP, Black, F-Bottom	Greiner	Cat# 781209
ELISA maxisorp microtiter plates	ThermoFisher	Cat# 439454
Concanavalin A (ConA)	Millipore Sigma	Cat# C2272
Blotting-grade Blocker (contains BSA)	Biorad	Cat# 1706404
Whey from bovine milk, spray dried	Millipore Sigma	Cat# W1500-2.5KG
Opti-MEM™ Reduced Serum medium	ThermoScientific	Cat# 31985070
Streptavidin horseradish peroxidase	Vector Laboratories	Cat# SA5004; RRID: AB_2336509
NativePAGE™ 20X Running Buffer	ThermoScientific	Cat# BN2001
Imidazole	Millipore Sigma	Cat# I5513-25G
Tween-20	Millipore Sigma	Cat# P7949
EconoPac disposable chromatography columns	Biorad	Cat# 7321010
PP Microplate 384 well, F-Shape, Black 128/85/15mm	Greiner	Cat# 781209
PBS (1X)	Corning	Cat# 21040-CV
HEPES	Millipore Sigma	Cat# H4034
Ampicillin sodium salt	Millipore Sigma	Cat# A9518
Kanamycn sulphate	Millipore Sigma	Cat# 60615
96-well Clear V-Bottom TC-treated Microplate	Corning	Cat# 3894
LIVE/DEAD™ Fixable Far Red Dead Cell Stain Kit, for 633 or 635 nm excitation	ThermoScientific	Cat# L34973
D_2O	Millipore Sigma	Cat# 151882
Formic Acid	Millipore Sigma	Cat# 27001
TritonX-100	Millipore Sigma	Cat# T9284
Uranyl formate	Electron Microscopy Sciences	Cat# 22451
neutralite-avidin peroxidase (N-HRP)	Southern Biotech	Cat# 7200-05
Critical commercial assays		
Pierce™ BCA Protein Assay Kit	ThermoScientific	Cat# 23227
KPL TMB Microwell Peroxidase Substrate System	SeraCare	Cat# 5120-0047
HIV-1 p24 ELISA Kit	Abcam	Cat# ab218268
britelite plus Reporter Gene Assay System	PerkinElmer	Cat# 6066761
Deposited data		

REAGENT or RESOURCE	SOURCE	IDENTIFIER
Native gel image of C.1086 variants	This Manuscript	https://doi.org/10.17632/9zp2hh598z.1
Experimental models: Cell lines		
FreeStyle 293F	Invitrogen	Cat# R79007; RRID: CVCL_D603
TZM-bl	NIH AIDS Reagent Program	Cat# 8129; RRID: CVCL_B478
HEK 293T	ATCC	Cat# CRL-3216; RRID: CVCL_0063
CEM-NK^{r} CCR5+	NIH AIDS Reagent Program	Cat# 4376; RRID: CVCL_X622
Experimental models: Organisms/strains		
Rabbit: New Zealand White female	Covance	N/A
Oligonucleotides		
N279Q_For 5′-CAAAATGCCAAAACAATAATAGTACAC-3′	This Manuscript	N/A
N279Q_Rev 5′-TGTCAGATTTTCAGATCTAATTATTATCTCTTC-3′	This Manuscript	N/A
N280D_For 5′-GATGCCAAAACAATAATAGTACACC-3′	This Manuscript	N/A
N280D_Rev 5′-GTTTGTCAGATTTTCAGATCTAATTATTATCTC-3′	This Manuscript	N/A
G459E_For 5′-GAGCAATCAAATGAAACAAATGACAC-3′	This Manuscript	N/A
G459_rev 5′-TCCATCACGTAGCAATAGTAGTC-3′	This Manuscript	N/A
G458Y_For 5′-TATGGTCAATCAAATGAAACAAATGAC-3′	This Manuscript	N/A
G458Y_Rev 5′-ATCACGTAGCAATAGTAGTCCTG-3′	This Manuscript	N/A
S365K_For 5′-AAAGGAGGGGATCTAGAAATTAC-3′	This Manuscript	N/A
S365K_Rev 5′-GGATGGTTCAAACTTTATTGTTTTACTAG-3′	This Manuscript	N/A
T162A_For 5′-GCGACGGAACTAAGAGATAAAAAAC-3′	This Manuscript	N/A
T162A_Rev 5′-TGCATTGAAAGAGCAATTTTTCATTACTTC-3′	This Manuscript	N/A
D167A_For 5′-GCGAAAAAACAAAAGGTGCAT-3′	This Manuscript	N/A
D167A_Rev 5′-TCTTAGTTCCGTGGTTGC-3′	This Manuscript	N/A
For_N156A 5′-GCATGCTCTTTCAATGCAACC-3′	This Manuscript	
Rev_156 5′-TTTCATTACTTCACTGGTGTCACTC-3′	This Manuscript	N/A
For_173A 5′-GCAGCGCTTTTTTATAAACTTGATGTAG-3′	This Manuscript	N/A
Rev_173 5′-CAATGCAACCACGGAACTAAG-3′	This Manuscript	N/A
For_181A 5′-GCAGTACCACTTAATGGAAACAG-3′	This Manuscript	N/A

REAGENT or RESOURCE	SOURCE	IDENTIFIER
Rev_181A 5′-ATCAAGTTTATAAAAAAGCGCATGCAC-3′	This Manuscript	N/A
Recombinant DNA		
pSV-A-MLV-env	NIH AIDS Reagent program	Cat# ARP-1065
pCDNA3.1_C.1086 K160N RQH S365K	This Manuscript	N/A
pCDNA3.1_C.1086 K160N RQH D167A	This Manuscript	N/A
pCDNA3.1_C.1086 K160N RQH G458Y	This Manuscript	N/A
pCDNA3.1_C.1086 K160N RQH N279Q	This Manuscript	N/A
pCDNA3.1_C.1086 K160N RQH T162A	This Manuscript	N/A
pCDNA3.1_C.1086 K160N RQH N280D	This Manuscript	N/A
pCDNA3.1_C.1086 K160N RQH G459E	This Manuscript	N/A
pCDNA3.1_C.1086 K160N RQH G459P	This Manuscript	N/A
pCDNA3.1_C.1086 K160N RQH	This Manuscript	N/A
pCDNA3.1_C.1086 K160N RQY	This Manuscript	N/A
pCDNA3.1_C.1086 K160N RQH I371A	This Manuscript	N/A
pCDNA3.1_C.1086 K160N RQH R166A	This Manuscript	N/A
pCDNA3.1_C.1086 K160N RQH N156A	This Manuscript	N/A
pCDNA3.1_C.1086 K160N RQH 611A	This Manuscript	N/A
pCDNA3.1_C.1086 K160N RQH 160A	This Manuscript	N/A
pCDNA3.1_C.1086 K160N RQH 160K	This Manuscript	N/A
pCDNA3.1_C.1086 K160N RQH 332A	This Manuscript	N/A
pCDNA3.1_C.1086 K160N RQH 181A	This Manuscript	N/A
pCDNA3.1_C.1086 K160N RQH 166K	This Manuscript	N/A
pCDNA3.1_C.1086 K160N RQH 173A	This Manuscript	N/A
pGA1_C.1086_WT_gp140	This Manuscript	N/A
pGA1_C.1086_NFL_gp140	This Manuscript	N/A
pGA1_C.1086_UFO_gp140	This Manuscript	N/A
pGA1_C.1086_UFO_v2_RHH_gp140	This Manuscript	N/A
pGA1_C.1086_UFO_v2_RHH_gp140	This Manuscript	N/A
pGA1_C.1086_UFO_v2-RQY_gp140	This Manuscript	N/A
pGA1_BG505_SOSIP_V2-HS mutants	This Manuscript	N/A
pGA1_C.1086_UFO_v2_V2-HS mutants	This Manuscript	N/A
pGA1_BG505_SOSIP_gp140	This Manuscript	N/A
pCDNA3.1_C.1086 K160N	Laboratory of Dr. Cynthia Derdeyn, Emory University (Burton et al., 2019)	N/A
Software and algorithms		
ForteBio Octet Data Analysis v9 software	ForteBio	N/A
ForteBio Data Acquisition v9	ForteBio	N/A
Prism v8	GraphPad	RRID:SCR_002798
FlowJo v10.8.0	FlowJo	RRID:SCR_008520
UCSF Chimera v1.14	Pettersen et al., 2004	RRID:SCR_004097

REAGENT or RESOURCE	SOURCE	IDENTIFIER
HIV Databases (Los Alamos)	http://www.hiv.lanl.gov/content/index	RRID:SCR_000614
CATNAP	https://www.hiv.lanl.gov/catnap	RRID:SCR_016170
Leginon software package	Suloway et al., 2005	RRID:SCR_016731
Appion package	Lander et al., 2009	RRID:SCR_016734
R Package	https://www.r-project.org/	RRID: SCR_001905
HD-Examiner	Sierra Analytics	N/A
HX-Express v2	Guttman et al., 2014, Weis et al., 2006	N/A
Other		
Anti-human Fc capture (AHC) Biosensors	ForteBio	Cat# 18-5060
FEI Tecnai Spirit T12 transmission electron microscope	Tecnai	N/A
Synapt G2-Si Q-TOF mass spectrometer	Waters	N/A
Octet RED384 System	ForteBio, Sartorius	N/A
Carbon coated Cu400 grid for NS-EM	Electron Microscopy Sciences	Cat# EMS400-CU